Application of Predictor Feedback to Compensate Time Delays in Connected Cruise Control

Tamás G. Molnár, Wubing B. Qin, Tamás Insperger, and Gábor Orosz

***Abstract*— In this paper, we investigate a vehicular string traveling on a single lane, where vehicles use connected cruise control to regulate their longitudinal motion based on data received from other vehicles via wireless vehicle-to-vehicle communication. Assuming digital controllers, the sample-and-hold units introduce time-periodic time delays in the control loops and the delays increase when data packets are lost. We investigate the effect of packet losses on plant and string stability while varying the control gains and determine the minimum achievable time gap below which stability cannot be achieved. We propose two predictor feedback control strategies that overcome the destabilizing effect of the time delay caused by the sample-and-hold unit and packet losses.**

***Index Terms*— Connected cruise control, predictive control, stability analysis, time delay.**

I. Introduction

FEEDBACK loops are always associated with certain time delays due to the finite speed of sensing, data processing, and actuation, and time delays are often considered to be the source of instability in dynamic systems. A promising way of stabilizing unstable time delay systems is the application of predictor feedback control strategies [1]. The main concept of predictor feedback is that the actual (delay-free) state of the system is predicted and used for feedback instead of the delayed state obtained from measurements or observers. The prediction can be based on the solution of an internal model of the dynamic system, which results in the so-called finite spectrum assignment (FSA) technique [2]–[5]. If the internal model is a perfect representation of the actual system, then the delay-free state can exactly be predicted, and a perfect implementation of the control law reduces the closed loop system to a delay-free system [2], [6]–[11]. This way, predictor feedback has the potential to stabilize systems with time delays.

Manuscript received January 12, 2017; revised April 4, 2017 and July 20, 2017; accepted September 15, 2017. Date of publication November 7, 2017; date of current version February 1, 2018. This work was supported by the U. S. National Science Foundation under Grant 1300319. The Associate Editor for this paper was P. Zingaretti. *(Corresponding author: Tamás G. Molnár.)*

T. G. Molnár is with the Department of Applied Mechanics, Budapest University of Technology and Economics, H-1111 Budapest, Hungary (e-mail: molnar@mm.bme.hu).

W. B. Qin and G. Orosz are with the Department of Mechanical Engineering, University of Michigan, Ann Arbor, MI 48109 USA (e-mail: wubing@umich.edu; orosz@umich.edu).

T. Insperger is with the Department of Applied Mechanics, Budapest University of Technology and Economics, H-1111 Budapest, Hungary, and also with the MTA-BME Lendület Human Balancing Research Group, H-1111 Budapest, Hungary (e-mail: insperger@mm.bme.hu).

Color versions of one or more of the figures in this paper are available online at http://ieeexplore.ieee.org.

Digital Object Identifier 10.1109/TITS.2017.2754240

Time delays play a crucial role in the dynamics of vehicular traffic. In the case of human-driven vehicles, the reaction time of the driver – ranging between $0.3 - 1.5$ [s] – is the most important source of time delay. This reaction time is often the source of instabilities in traffic flow and may lead to congestion or even cause accidents on the road. Since improving safety and mobility of vehicular traffic is a major concern today [12], advanced driver assistance systems (ADAS) were developed to overcome these problems. ADAS must satisfy two stability criteria with regards to the longitudinal dynamics of the vehicles. On one hand, plant stability must be guaranteed, which is associated with safe driving along a prescribed velocity profile. On the other hand, when a group of vehicles forms a vehicular string, congestion waves traveling upstream the traffic flow must be attenuated that is referred as string stability [13]. String instability typically leads to the formation of stop-and-go traffic jams [14], [15] that impacts mobility negatively.

Several strategies have been proposed in the literature to ensure plant and string stability. When using adaptive cruise control (ACC), the vehicle is equipped with radars or cameras to measure the distance headway and the velocity difference between the vehicle and the preceding vehicle [16]. The sensors used in ACC strategy may be supported (or substituted) by wireless vehicle-to-vehicle (V2V) communication that enables the vehicle to monitor the vehicle ahead even when it is beyond the line of sight. (Note that the headway and the velocity difference can also be calculated from GPS signals.) V2V communication may also improve the safety and mobility of traffic by providing information about multiple vehicles ahead [17], [18]. In cooperative adaptive cruise control (CACC), the members of a vehicular string are equipped with ACC, but also obtain information about the motion of a designated platoon leader using communication [19]–[21]. However, in real traffic situations, not all vehicles are equipped with range sensors and since the range of V2V communication is limited, the data about leader's motion might not be accessible to every member of the vehicular string. Therefore, the concept of connected cruise control (CCC) was introduced in [18], [22], and [23], where all available V2V signals are utilized. This concept is applicable even in the presence of human-driven vehicles in the string and it can be used in realistic traffic scenarios. CCC can be used to support human drivers, to supplement sensory information, or to control the longitudinal motion of the vehicle.

In this paper, we investigate an application of the CCC concept while taking into account the intermittency in

V2V communication. For example, dedicated short range communication (DSRC) devices typically use the sampling period 100 [ms] to process the data during communication [24]–[26]. The sample-and-hold units used in digital controllers utilizing DSRC information introduce time-varying time delays into the control loop [27]. Disturbances during communication may lead to loss of data packets, which increases the time delay [28]. In this paper, we investigate the dynamics of vehicular strings when the communication is subject to deterministic packet loss scenarios. We investigate plant and string stability while varying the control gains for different numbers of consecutive packet losses and summarize our results using stability charts. We also show that the time delay gives a fundamental limit to the minimum achievable time gap, that is, to the maximum achievable flux in the traffic flow. The destabilizing effect of time delay on vehicle platoons was also demonstrated in [18], [23], and [27]–[32].

The main contributions of this paper are two predictor feedback control strategies that eliminate the destabilizing effect of the time-varying time delay. The first strategy estimates the velocity and the distance of the vehicles based on the last available data packets without requiring knowledge about the dynamics of the vehicular string. Such prediction can be done based on the history of GPS position and velocity contained by basic safety messages (BSM) [24]–[26]. The second strategy can be considered as an application of the FSA technique to a discrete-time system [4], [33]. This requires a dynamic model of the vehicles as the predicted state is obtained by the integration of the model. We show that the predictors may improve stability under intermittent communication and ensure robustness against the variations of time delay due to packet losses. Trade-off regarding using different predictors is also pointed out.

The outline of the paper is the following. Section II introduces the model of the vehicular string where the vehicles are driven by CCC. In Section III, we analyze the effects of the sample-and-hold units when digital controllers are used by members of the vehicular string. In Section IV, we carry out plant and string stability analysis. Section V demonstrates the effect of packet losses in wireless communication. In Sections VI and VII, we introduce two predictor feedback control strategies to overcome the destabilizing effect of packet losses and to compensate the processing delay of the digital controller. Finally, we draw conclusions in Section VIII.

II. Connected Cruise Control

In this paper, we consider a vehicular string on a single lane as shown in Fig. 1. We assume identical vehicles such that the motion of each member is controlled based on the position and velocity data received from the vehicle immediately ahead. This way, the analysis of the vehicular string can be simplified to the analysis of the leader-follower configuration at the bottom of Fig. 1. The headway h, the leader's velocity v_{L}, and the follower's velocity v_{F} satisfy

$$\dot{h}(t) = v_{\mathrm{L}}(t) - v_{\mathrm{F}}(t). \tag{1}$$

We assume that the follower's acceleration can be adjusted directly by the controller:

$$\dot{v}_{\mathrm{F}}(t) = a_{\mathrm{des}}(t), \tag{2}$$

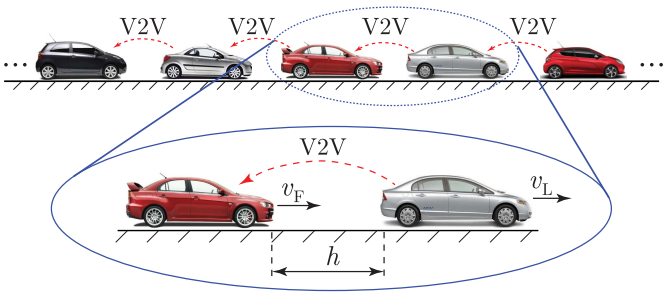

Fig. 1. String of connected vehicles traveling on a single lane. The vehicular string can be considered as the concatenation of the leader-follower pattern shown below. The red dashed arrows indicate wireless vehicle-to-vehicle communication.

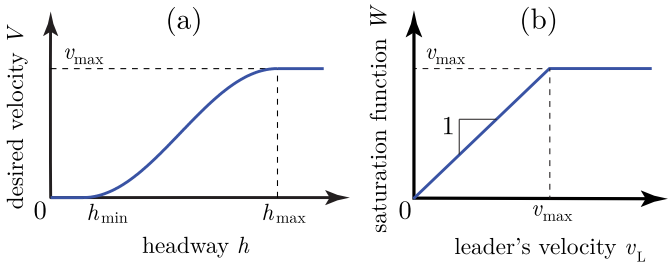

Fig. 2. (a) The desired velocity (4)-(5) as a function of the headway. (b) The saturation function (6).

where $a_{\mathrm{des}}(t)$ denotes the control input. We use a proportional-velocity (PV) controller widely used in the literature [18], [30]:

$$a_{\mathrm{des}}(t) = \alpha\left(V\big(h(t)\big) - v_{\mathrm{F}}(t)\right) + \beta\left(W\big(v_{\mathrm{L}}(t)\big) - v_{\mathrm{F}}(t)\right). \tag{3}$$

Here α and β denote the control gains, $V(h)$ is the follower's desired velocity that depends on the headway, and $W(v_{\mathrm{L}})$ is a saturation function. Note that several other control strategies also exist [22], [34]–[43] and the analysis carried out in this paper can also be applied to those controllers.

The controller (3) contains the range policy

$$V(h) = \begin{cases} 0 & \text{if } h \le h_{\min}, \\ F(h) & \text{if } h_{\min} < h < h_{\max}, \\ v_{\max} & \text{if } h \ge h_{\max}. \end{cases} \tag{4}$$

This states that the follower intends to stop if the headway drops below the limit $h_{\min}$. Once the headway exceeds the limit $h_{\max}$, the follower wants to travel with the maximum speed $v_{\max}$ allowed by road traffic regulations. Between these limits, the desired velocity increases monotonously according to the function $F(h)$. We prescribe $F(h_{\min}) = 0$, $F(h_{\max}) = v_{\max}$, $F'(h_{\min}) = F'(h_{\max}) = 0$ in order to achieve smooth velocity and acceleration profiles. As an example, we satisfy these conditions by the choice

$$F(h) = \frac{v_{\max}}{2}\left(1 - \cos\left(\pi\,\frac{h - h_{\min}}{h_{\max} - h_{\min}}\right)\right), \tag{5}$$

see Fig. 2(a). Note that any other monotonous and sufficiently smooth function $F(h)$ could be used as well. Besides, other range policies also exist, see [23], [34], [44]–[46].

When the leader's velocity exceeds the maximum speed $v_{\max}$ allowed by road traffic regulations, we switch off the connected cruise control. We realize this by the saturation

function

$$W(v_{\mathrm{L}}) = \begin{cases} v_{\mathrm{L}} & \text{if } v_{\mathrm{L}} \le v_{\max}, \\ v_{\max} & \text{if } v_{\mathrm{L}} > v_{\max}, \end{cases} \tag{6}$$

that is displayed in Fig. 2(b).

From this point on, we assume $v_{\mathrm{L}} \le v_{\max}$, where system (1), (2), (3) has a unique equilibrium

$$V(h^*) = v_{\mathrm{F}}^* = v_{\mathrm{L}}^*. \tag{7}$$

This equilibrium represents the desired uniform flow, where each member of the vehicular string travels with the same constant velocity $V(h^*)$ while keeping a constant headway h^*. The control gains α and β must be chosen such that we guarantee the stability of the equilibrium.

III. Application of a Digital Controller

We assume that a digital controller is implemented to realize the control law (3), thus the headway h, the leader's velocity v_{L}, and the follower's velocity v_{F} are sampled with sampling period Δt. For dedicated short range communication (DSRC) devices, the typical sampling period is $\Delta t = 100$ [ms]. We assume that the clocks of the leader and the follower are synchronized, which can be achieved using satellites. Thus, all headway and velocity data is available at the same discrete time instants $t_k = k\Delta t$. Note that it takes a certain amount of time for the leader to process the sensed data and to transmit it, and for the follower to receive data, to process it, and to use it for actuating the vehicle. Therefore, at time instant t_k, the controller is able to use the data measured at the previous sampling instant t_{k-1}. This implies that the controller has a certain processing delay. The control input is held constant by a zero-order-hold (ZOH) unit along $[t_k, t_{k+1})$. Therefore, when a digital controller is implemented, the control law (2) modifies to

$$\dot{v}_{\mathrm{F}}(t) = a_{\mathrm{des}}(t_{k-1}), \quad t \in [t_k, t_{k+1}), \tag{8}$$

where a_{des} is given by (3). Equations (1), (3), (8) define a continuous-time nonlinear system with piecewise constant input. Correspondingly, the processing delay introduced by the ZOH is time-periodic as shown in Fig. 3(a). During each sampling period, the time delay increases linearly from Δt, since $a_{\mathrm{des}}(t_{k-1})$ is used at t_k, to $2\Delta t$, since $a_{\mathrm{des}}(t_{k-1})$ is still used at t_{k+1}. Note that since delayed states are available for the follower instead of actual ones, there is a possibility to improve control performance by estimating the actual state via predictors, which will be discussed further below.

According to [47], the dynamics (1), (3), (8) can be converted to a discrete-time map. In particular, we solve the system along $t \in [t_k, t_{k+1})$ with the initial conditions at t_k, which gives

$$\begin{bmatrix} h(k+1) \\ v_{\mathrm{F}}(k+1) \end{bmatrix} = \begin{bmatrix} 1 & -\Delta t \\ 0 & 1 \end{bmatrix} \begin{bmatrix} h(k) \\ v_{\mathrm{F}}(k) \end{bmatrix} + \begin{bmatrix} -\frac{1}{2}\alpha \Delta t^2 \\ \alpha \Delta t \end{bmatrix} V\big(h(k-1)\big)$$

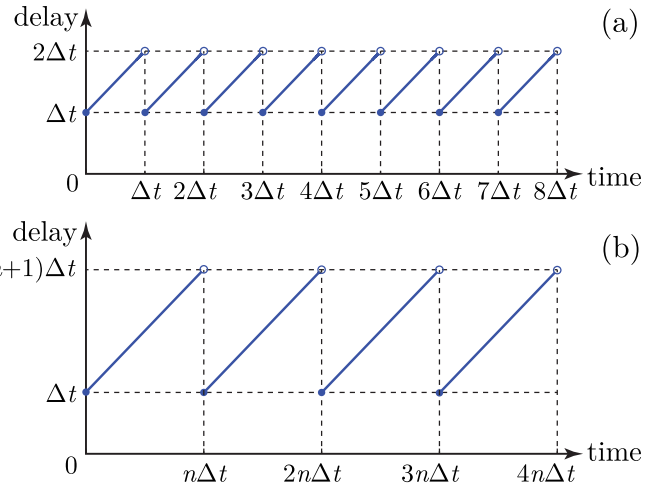

Fig. 3. The time delay caused by digital control: (a) without packet losses, (b) when every n-th packet is received.

$$+ \begin{bmatrix} 0 & \frac{1}{2}(\alpha+\beta)\Delta t^2 \\ 0 & -(\alpha+\beta)\Delta t \end{bmatrix} \begin{bmatrix} h(k-1) \\ v_{\mathrm{F}}(k-1) \end{bmatrix} + \begin{bmatrix} -\frac{1}{2}\beta \Delta t^2 \\ \beta \Delta t \end{bmatrix} W\big(v_{\mathrm{L}}(k-1)\big) + \begin{bmatrix} \int_{t_k}^{t_{k+1}} v_{\mathrm{L}}(t)\mathrm{d}t \\ 0 \end{bmatrix}, \tag{9}$$

where $h(k) = h(t_k)$, $v_{\mathrm{F}}(k) = v_{\mathrm{F}}(t_k)$, $v_{\mathrm{L}}(k) = v_{\mathrm{L}}(t_k)$.

The stability of the uniform flow equilibrium (7) of system (1), (3), (8) is equivalent to the stability of the fixed point of the discrete-time map (9). Here, we restrict ourselves to linear analysis, therefore we linearize (9), which gives

$$\begin{bmatrix} \tilde{h}(k+1) \\ \tilde{v}_{\mathrm{F}}(k+1) \end{bmatrix} = \begin{bmatrix} 1 & -\Delta t \\ 0 & 1 \end{bmatrix} \begin{bmatrix} \tilde{h}(k) \\ \tilde{v}_{\mathrm{F}}(k) \end{bmatrix} + \begin{bmatrix} -\frac{1}{2}\alpha V'(h^*)\Delta t^2 & \frac{1}{2}(\alpha+\beta)\Delta t^2 \\ \alpha V'(h^*)\Delta t & -(\alpha+\beta)\Delta t \end{bmatrix} \begin{bmatrix} \tilde{h}(k-1) \\ \tilde{v}_{\mathrm{F}}(k-1) \end{bmatrix} + \begin{bmatrix} -\frac{1}{2}\beta \Delta t^2 \\ \beta \Delta t \end{bmatrix} \tilde{v}_{\mathrm{L}}(k-1) + \begin{bmatrix} \int_{t_k}^{t_{k+1}} \tilde{v}_{\mathrm{L}}(t)\mathrm{d}t \\ 0 \end{bmatrix}, \tag{10}$$

where $\tilde{h}(t)$, $\tilde{v}_{\mathrm{L}}(t)$, and $\tilde{v}_{\mathrm{F}}(t)$ denote small fluctuations around the equilibrium headway h^* and equilibrium velocity $V(h^*)$ given by (7). From (4), the derivative $V'(h^*)$ reads

$$V'(h^*) = \begin{cases} 0 & \text{if} h^* \le h_{\min}, \\ F'(h^*) & \text{if} h_{\min} < h^* < h_{\max}, \\ 0 & \text{if} h^* \ge h_{\max}. \end{cases} \tag{11}$$

We assume sinusoidal fluctuations in leader's velocity,

$$\tilde{v}_{\mathrm{L}}(t) = v_{\mathrm{L}}^{\mathrm{amp}} \sin(\omega t), \tag{12}$$

since real fluctuations can be considered as an infinite sum of harmonic functions. This way, the integral in (10) can be written in the form

$$\int_{t_k}^{t_{k+1}} \tilde{v}_{\mathrm{L}}(t)\mathrm{d}t = \beta_0 \tilde{v}_{\mathrm{L}}(t_k) + \beta_2 \tilde{v}_{\mathrm{L}}(t_{k-2}), \tag{13}$$

where

$$\beta_0 = \frac{\cos(2\omega\Delta t) - \cos(3\omega\Delta t)}{\omega \sin(2\omega\Delta t)}, \quad \beta_2 = \frac{\cos(\omega\Delta t) - 1}{\omega \sin(2\omega\Delta t)}. \quad (14)$$

If we define the state, the input, and the output of the linear system (10) as

$$\mathbf{x}(k) = \begin{bmatrix} \tilde{h}(k) \\ \tilde{v}_{\mathrm{F}}(k) \end{bmatrix}, \quad u(k) = \tilde{v}_{\mathrm{L}}(k), \ y(k) = \tilde{v}_{\mathrm{F}}(k), \quad (15)$$

we can rewrite (10), (12) in the form

$$\begin{aligned} \mathbf{x}(k+1) &= \mathbf{a}_0\,\mathbf{x}(k) + \mathbf{a}_1\,\mathbf{x}(k-1) \\ &\quad + \mathbf{b}_0\,u(k) + \mathbf{b}_1\,u(k-1) + \mathbf{b}_2\,u(k-2), \\ y(k) &= \mathbf{c}\,\mathbf{x}(k), \end{aligned} \quad (16)$$

where

$$\mathbf{a}_0 = \begin{bmatrix} 1 & -\Delta t \\ 0 & 1 \end{bmatrix}, \quad \mathbf{a}_1 = \begin{bmatrix} -\frac{1}{2}\alpha V'(h^*)\Delta t^2 & \frac{1}{2}(\alpha+\beta)\Delta t^2 \\ \alpha V'(h^*)\Delta t & -(\alpha+\beta)\Delta t \end{bmatrix},$$

$$\mathbf{b}_0 = \begin{bmatrix} \beta_0 \\ 0 \end{bmatrix}, \quad \mathbf{b}_1 = \begin{bmatrix} -\frac{1}{2}\beta\Delta t^2 \\ \beta\Delta t \end{bmatrix}, \ \mathbf{b}_2 = \begin{bmatrix} \beta_2 \\ 0 \end{bmatrix}, \ \mathbf{c} = \begin{bmatrix} 0 & 1 \end{bmatrix}. \quad (17)$$

Now we introduce the augmented state vector

$$\mathbf{X}(k) = \begin{bmatrix} \mathbf{x}(k) \\ \mathbf{x}(k-1) \end{bmatrix}, \quad (18)$$

such that (16) is written in the state-space representation

$$\begin{aligned} \mathbf{X}(k+1) &= \mathbf{A}_1\mathbf{X}(k) + \mathbf{B}_0 u(k) + \mathbf{B}_1 u(k-1) + \mathbf{B}_2 u(k-2), \\ y(k) &= \mathbf{C}_1\mathbf{X}(k). \end{aligned} \quad (19)$$

Here the system, the input, and the output matrices read

$$\mathbf{A}_1 = \begin{bmatrix} \mathbf{a}_0 & \mathbf{a}_1 \\ \mathbf{I} & \mathbf{0} \end{bmatrix}, \quad \mathbf{B}_0 = \begin{bmatrix} \mathbf{b}_0 \\ \mathbf{o} \end{bmatrix}, \ \mathbf{B}_1 = \begin{bmatrix} \mathbf{b}_1 \\ \mathbf{o} \end{bmatrix}, \ \mathbf{B}_2 = \begin{bmatrix} \mathbf{b}_2 \\ \mathbf{o} \end{bmatrix},$$
$$\mathbf{C}_1 = \begin{bmatrix} \mathbf{c} & \mathbf{o}^{\mathrm{T}} \end{bmatrix}, \quad (20)$$

where $\mathbf{0} \in \mathbb{R}^{2\times 2}$ and $\mathbf{I} \in \mathbb{R}^{2\times 2}$ are the zero and the identity matrices, respectively, $\mathbf{o} \in \mathbb{R}^2$ denotes the zero vector, and T stands for transpose.

IV. Plant and String Stability

When applying connected cruise control for vehicular strings, two stability criteria – plant and string stability – must be fulfilled. Plant stability is related to the safety and collision avoidance between vehicles, whereas string stability is associated with disturbance attenuation along vehicular strings and ensuring smooth traffic flow. We present the stability analysis of (19) in this section following the method shown in [27].

The system is plant stable if the follower is able to approach leader's constant velocity v_{L}^*. In the absence of fluctuations in the leader's velocity ($\tilde{v}_{\mathrm{L}}(t) \equiv 0$, $u(k) = 0$), the linear map (19) simplifies to

$$\mathbf{X}(k+1) = \mathbf{A}_1\mathbf{X}(k). \quad (21)$$

Plant stability is guaranteed if all eigenvalues of $\mathbf{A}_1$ lie within the unit circle in the complex plane. The eigenvalues are given by the characteristic equation

$$\det(z\mathbf{I} - \mathbf{A}_1) = 0. \quad (22)$$

Plant stability can be lost in three qualitatively different ways: an eigenvalue crosses the unit circle at 1, an eigenvalue crosses the unit circle at -1, a pair of complex conjugate eigenvalues crosses the unit circle. The first case leads to a non-oscillatory stability loss, while the last two lead to oscillatory stability loss. The corresponding plant stability boundaries are obtained for $z = 1$, or $z = -1$, or $z = \mathrm{e}^{\pm \mathrm{i}\theta}$ ($\mathrm{i}^2 = -1$, $\theta \in (0, \pi)$). Substituting $z = 1$ and $z = -1$ into (22) while using (17) and (20), we get the plant stability boundaries in the form

$$\alpha = 0, \quad (23)$$

$$\alpha = -\frac{2}{\Delta t} - \beta, \quad (24)$$

respectively. Substituting $z = \mathrm{e}^{\mathrm{i}\theta}$ into (22) while using (17) and (20), and separating the real and the imaginary parts, we obtain the third plant stability boundary parameterized by $\theta \in (0, \pi)$:

$$\begin{aligned} \alpha &= \frac{4\sin^2\theta + 6\cos\theta - 6}{V'(h^*)\Delta t^2}, \\ \beta &= \frac{2\sin^2\theta + \cos\theta - 1}{\Delta t} - \frac{4\sin^2\theta + 6\cos\theta - 6}{V'(h^*)\Delta t^2}. \end{aligned} \quad (25)$$

Fig. 4(a) shows the plant stability boundaries in the plane (β, α). We used $h_{\min} = 5$ [m], $h_{\max} = 35$ [m], $v_{\max} = 30$ [m/s] to define the range policy, and investigated the uniform flow equilibrium given by $h^* = 20$ [m], $v_{\mathrm{L}}^* = v_{\mathrm{F}}^* = 15$ [m/s], which imply $V'(h^*) = \pi/2$ [1/s]. We keep these parameters fixed throughout the paper. The dashed, the dotted, and the solid red lines correspond to the plant stability boundaries associated with $z = 1$, $z = -1$, and $z = \mathrm{e}^{\mathrm{i}\theta}$, respectively. They enclose the light gray-shaded plant stable domain. The eigenvalue plots in Fig 4(b) show the eigenvalues of matrix $\mathbf{A}_1$ for different plant stability losses (cases A, B, and C) and for a plant stable scenario (case D).

The system is string stable, if the follower is able to attenuate fluctuations in the leader's velocity. This implies restrictions on the amplification from input to output. Therefore, we calculate the transfer function corresponding to (19) using Z transform, which gives

$$\Gamma(z) = \mathbf{C}_1(z\mathbf{I} - \mathbf{A}_1)^{-1}\left(\mathbf{B}_2 z^{-2} + \mathbf{B}_1 z^{-1} + \mathbf{B}_0\right). \quad (26)$$

The corresponding magnitude ratio is

$$M(\omega) = \left|\Gamma\left(\mathrm{e}^{\mathrm{i}\omega\Delta t}\right)\right|, \quad (27)$$

and the detailed formula of $M(\omega)$ is given by (66)-(67) in Appendix. The necessary and sufficient condition for string stability is given by

$$M(\omega) < 1, \quad \forall\ \omega > 0. \quad (28)$$

String stability may be lost in different frequency domains as the maximum of $M(\omega)$ goes above 1. Considering ω_{cr} to be the critical frequency where string stability is lost, three kinds of string stability boundaries can be distinguished: $\omega_{\mathrm{cr}} = 0$, $\omega_{\mathrm{cr}} = (2k+1)\pi/\Delta t$ with $k \in \mathbb{N}$, and when ω_{cr} is not equal to either of these. Since $M(0) = 1$ and $M'(0) = \mathrm{d}M/\mathrm{d}\omega\,(0) = 0$

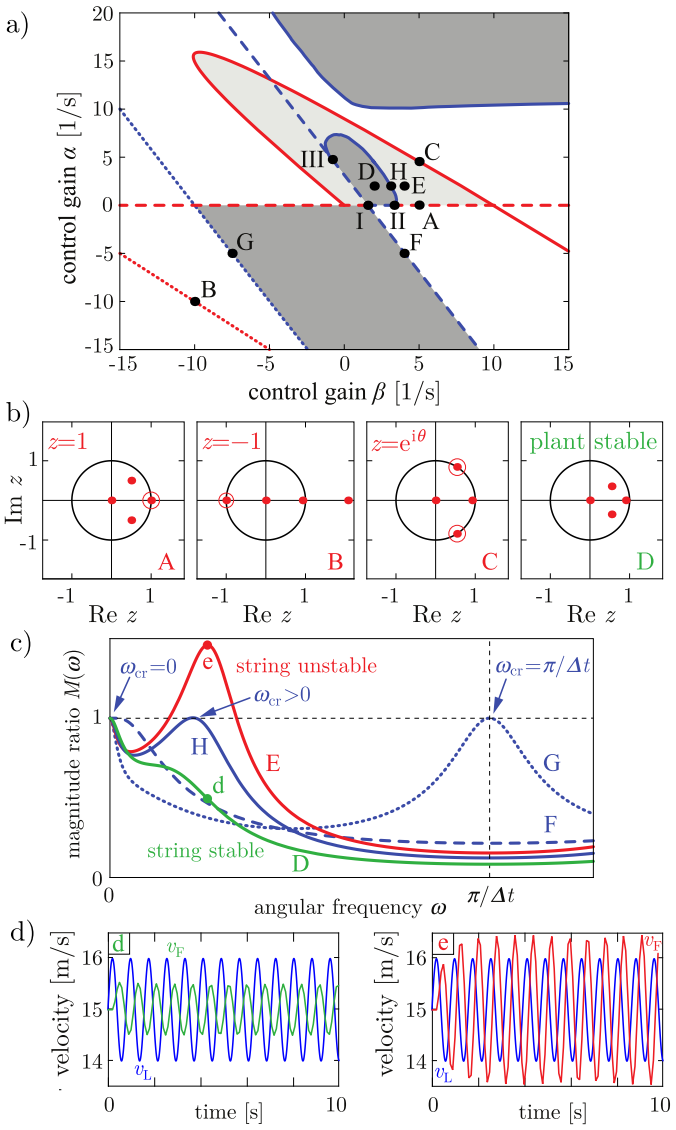

Fig. 4. (a) Stability chart in the (β, α)-plane of the control gains for $\Delta t = 100$ [ms]. Red and blue lines indicate plant and string stability boundaries, respectively, whereas the light gray region is plant stable, the dark gray region is string stable. (b) The eigenvalues of the system matrix $\mathbf{A}_1$ corresponding to points A-D. (c) The magnitude ratio $M(\omega)$ corresponding to points D-H. The intersection points I, II, and III in panel (a) are used when deriving the critical sampling time $\Delta t_{\rm cr}$. (d) Numerical simulations corresponding to points d and e.

always hold, the string stability boundaries for $\omega_{\rm cr} = 0$ are given by $M''(0) = 0$, which yields

$$\alpha = 0, \tag{29}$$

$$\alpha = \frac{2\left(V'(h^*) - \beta\right)}{1 - \left(V'(h^*)\right)^2 \Delta t^2/6}. \tag{30}$$

At $\omega_{\rm cr} = (2k+1)\pi/\Delta t$, condition $M(\omega_{\rm cr}) = 1$ gives the string stability boundary

$$\beta = \left(\left(\frac{V'(h^*)^2 \Delta t^2}{(2k+1)^2\pi^2} - 1\right)\alpha^2 - \frac{4}{\Delta t}\alpha - \frac{4}{\Delta t^2}\right)\frac{1}{2\alpha + 4/\Delta t}. \tag{31}$$

For $\omega_{\rm cr} > 0$, $\omega_{\rm cr} \neq (2k+1)\pi/\Delta t$, equations

$$M(\omega_{\rm cr}) = 1, \quad M'(\omega_{\rm cr}) = 0 \tag{32}$$

define the string stability boundary, which can be obtained numerically when varying the parameter $\omega_{\rm cr}$.

In Fig. 4(a), dashed, dotted, and solid blue lines indicate string stability boundaries for $\omega_{\rm cr} = 0$, $\omega_{\rm cr} = (2k+1)\pi/\Delta t$, and $\omega_{\rm cr} > 0$, $\omega_{\rm cr} \neq (2k+1)\pi/\Delta t$, respectively. The string stable regions are shaded as dark gray, while the magnitude ratios $M(\omega)$ are depicted in Fig. 4(c) for different string stability losses (cases F, G, and H), for a string stable scenario (case D), and a string unstable scenario (case E). Fig. 4(d) shows numerical simulations for a string stable and a string unstable case corresponding to points d and e in Fig. 4(c), respectively. Note that the string but not plant stable regions at the top and the bottom of Fig. 4(a) are physically irrelevant, hence we do not depict them in what follows. Accordingly, the dotted stability boundaries corresponding to $z = -1$ and $\omega_{\rm cr} = (2k+1)\pi/\Delta t$ cannot be observed experimentally. When designing the controller, the gains α and β should be chosen from the intersection of the plant and string stable domains in order to guarantee safe driving and smooth traffic flow.

The sampling time Δt has a significant effect on the size of the plant and string stable region. If we increase Δt, the time delay of the system increases and the stable region becomes smaller. The stable region disappears at the critical case

$$\Delta t_{\rm cr} = \frac{1}{3V'(h^*)}, \tag{33}$$

where in Fig. 4(a) the three intersection points marked by I, II, III coincide. The derivation of (33) is discussed in Appendix in detail. Assuming $V'(h^*) = \pi/2$ [1/s], we get $\Delta t_{\rm cr} = 212$ [ms] for the critical sampling period. If a larger sampling time is used, $\Delta t > \Delta t_{\rm cr}$, the stable region disappears, and no pair of control gains (β, α) can guarantee both plant and string stability. Note that $T_{\rm h} = 1/V'(h^*)$ can be interpreted as the time gap between the leader and follower. Thus, (33) gives a fundamental limit how close the vehicles can travel to each other for a given Δt and determines the maximum achievable flux in the traffic flow.

We also remark that one may approximate the time-varying time delay by its average $\bar\tau$. Thus, the continuous-time approximation of (3), (8) reads

$$a_{\rm des}(t) = \alpha\left(V\left(h(t-\bar\tau)\right) - v_{\rm F}(t-\bar\tau)\right) + \beta\left(W\left(v_{\rm L}(t-\bar\tau)\right) - v_{\rm F}(t-\bar\tau)\right). \tag{34}$$

The effect of this control law was analyzed in [18], where the critical time delay was shown to be $\bar\tau_{\rm cr} = 1/(2V'(h^*))$, which is in agreement with (33) considering that $\bar\tau = 3/2\,\Delta t$, see Fig. 3(a).

V. Packet Losses in Vehicle-to-Vehicle Communication

As mentioned above, when using wireless vehicle-to-vehicle communication in real traffic situations, data is transmitted intermittently. Moreover, some data packets sent by one member of the vehicular string may not reach other vehicles. Consequently, the most recent data about the leader's velocity and headway may not be available for the controller of the

follower and the controller must use the data from previously delivered packets. That is, packet losses increase the effective time delay in the control loop that has a significant adverse effect on stability [28]. Here we analyze the effect of such packet losses.

We assume that only the leader's velocity and the headway data is subject to packet loss, since the follower's velocity is measured on board and is available at each time step. During the analysis, we restrict ourselves to cases where packet losses occur in a deterministic fashion. Note, however, that in real traffic, the packet losses occur in a stochastic manner, which yields stochastically varying time delays. For the analysis of systems with stochastic delays, the reader is referred to [28] and [48]. Nevertheless, assuming deterministic packet loss scenarios is only considered to simplify the analysis, while the predictor can also be used in the case of stochastic packet loss scenarios.

Let us assume that the communication suffered $\tau(k)-1$ consecutive packet losses up to the k-th time instant, i.e., the last headway and leader's velocity data was delivered $\tau(k)$ time steps earlier. Thus, using the controller (3) we obtain

$$\begin{aligned} \dot{v}_{\mathrm{F}}(t) &= a_{\mathrm{des}}(t_{k-1}), \quad t \in [t_k, t_{k+1}), \\ a_{\mathrm{des}}(t_{k-1}) &= \alpha \left(V\big(h(t_{k-\tau(k)})\big) - v_{\mathrm{F}}(t_{k-1}) \right) \\ &\quad + \beta \left(W\big(v_{\mathrm{L}}(t_{k-\tau(k)})\big) - v_{\mathrm{F}}(t_{k-1}) \right). \end{aligned} \tag{35}$$

Note that by substituting $\tau(k)=1$ (corresponding to no packet loss), we get back (3), (8).

According to (35), the packet losses increase the effective time delay in the system, which is demonstrated in Fig. 3 for the case where every n-th packet is received periodically. The time delay associated with the leader's velocity and the headway data is $n\Delta t$-periodic and increases from Δt to $(n+1)\Delta t$ in each period as shown in Fig. 3(b). This way, the principal period of the system becomes $n\Delta t$. Note, however, that the follower's velocity is not subject to packet losses, and its time delay is still varying between Δt and $2\Delta t$ as shown in Fig. 3(a).

In order to analyze the dynamics and stability properties of (1), (35), we integrate the equations along $[t_k, t_{k+1})$ and assume the sinusoidal fluctuations (12) in the leader's velocity. After linearization we get the discrete-time map

$$\begin{aligned} \mathbf{x}(k+1) &= \mathbf{a}_0\,\mathbf{x}(k) + \tilde{\mathbf{a}}_1\,\mathbf{x}(k-1) + \tilde{\mathbf{a}}_\tau\,\mathbf{x}(k-\tau(k)) \\ &\quad + \mathbf{b}_0\,u(k) + \mathbf{b}_2\,u(k-2) + \mathbf{b}_\tau\,u(k-\tau(k), \\ y(k) &= \mathbf{c}\,\mathbf{x}(k), \end{aligned} \tag{36}$$

which is similar to (16) that governs the follower's motion in the absence of packet losses. Matrices $\mathbf{a}_0$, $\mathbf{b}_0$, $\mathbf{b}_2$, $\mathbf{c}$ are the same as defined in (17), whereas the others read

$$\begin{aligned} \tilde{\mathbf{a}}_1 &= \begin{bmatrix} 0 & \frac{1}{2}(\alpha+\beta)\Delta t^2 \\ 0 & -(\alpha+\beta)\Delta t \end{bmatrix}, \quad \tilde{\mathbf{a}}_\tau = \begin{bmatrix} -\frac{1}{2}\alpha V'(h^*)\Delta t^2 & 0 \\ \alpha V'(h^*)\Delta t & 0 \end{bmatrix}, \\ \mathbf{b}_\tau &= \mathbf{b}_1. \end{aligned} \tag{37}$$

Note that the matrix $\mathbf{a}_1$ given by (17) splits into two parts as $\mathbf{a}_1 = \tilde{\mathbf{a}}_1 + \tilde{\mathbf{a}}_\tau$, where $\tilde{\mathbf{a}}_1$ is associated with the follower's velocity unaffected by packet losses, and $\tilde{\mathbf{a}}_\tau$ is related to the headway subjected to packet loss. The effect of losing the leader's velocity data is represented by the term $u(k-\tau(k))$ in (36).

Let $n-1$ denote the maximum number of consecutive packet losses, i.e., assume that in the worst case scenario the controller needs to wait n sampling periods for a new data packet to arrive. Then, the discrete time delay $\tau(k)$ increases from 1 to n during the sampling periods. Choosing the size of the state vector according to n, system (36) can be represented in augmented state-space form by

$$\begin{aligned} \mathbf{X}(k+1) &= \mathbf{A}_{\tau(k)}\mathbf{X}(k) + \mathbf{B}_0 u(k) + \mathbf{B}_2 u(k-2) \\ &\quad + \mathbf{B}_\tau u(k-\tau(k)), \\ y(k) &= \mathbf{C}_\tau \mathbf{X}(k), \end{aligned} \tag{38}$$

where

$$\begin{aligned} \mathbf{X}(k) &= \begin{bmatrix} \mathbf{x}(k) \\ \mathbf{x}(k-1) \\ \vdots \\ \mathbf{x}\big(k-n\big) \end{bmatrix}, \quad \mathbf{B}_0 = \begin{bmatrix} \mathbf{b}_0 \\ \mathbf{o} \\ \vdots \\ \mathbf{o} \end{bmatrix}, \\ \mathbf{B}_2 &= \begin{bmatrix} \mathbf{b}_2 \\ \mathbf{o} \\ \vdots \\ \mathbf{o} \end{bmatrix}, \quad \mathbf{B}_\tau = \begin{bmatrix} \mathbf{b}_\tau \\ \mathbf{o} \\ \vdots \\ \mathbf{o} \end{bmatrix}, \\ \mathbf{A}_{\tau(k)} &= \begin{bmatrix} \mathbf{a}_0 & \tilde{\mathbf{a}}_1 & \mathbf{0} & \cdots & \mathbf{0} & \tilde{\mathbf{a}}_\tau & \mathbf{0} & \cdots & \mathbf{0} & \mathbf{0} \\ \mathbf{I} & \mathbf{0} & & & \cdots & & & & \mathbf{0} & \mathbf{0} \\ \mathbf{0} & \mathbf{I} & & & \cdots & & & & \mathbf{0} & \mathbf{0} \\ \vdots & \vdots & & & \ddots & & & & \vdots & \vdots \\ \mathbf{0} & \mathbf{0} & & & \cdots & & & & \mathbf{I} & \mathbf{0} \end{bmatrix}, \\ \mathbf{C}_\tau &= \begin{bmatrix} \mathbf{c} & \mathbf{o}^{\mathrm{T}} & \cdots & \mathbf{o}^{\mathrm{T}} \end{bmatrix}, \end{aligned} \tag{39}$$

cf. (18), (19), (20). Note that matrices $\mathbf{A}_{\tau(k)}$, $\mathbf{B}_0$, $\mathbf{B}_\tau$, $\mathbf{B}_2$, and $\mathbf{C}_\tau$ consist of $n+1$ blocks in each row or column and $\tilde{\mathbf{a}}_\tau$ is located in the $\tau(k)+1$-st column, i.e., it changes its location at each time step based on the value of the delay. As mentioned above, we restrict ourselves to the analysis of deterministic packet loss scenarios when every n-th packet is received periodically.

In order to analyze plant and string stability, the evolution of the system must be described by a discrete-time map along the principal period $n\Delta t$ [49]. We construct this map by applying n successive maps at each step of the period. If the packets are received at the k-th and the $(k+n)$-th time instant, the evolution of the system along $\big[k\Delta t,\ (k+n)\Delta t\big)$ is governed by map (38) with increasing delay in each step. Therefore, we use map (38) n times successively assuming $\tau(k)=1$, $\tau(k+1)=2$, …, $\tau(k+n-1)=n$, respectively, which yields

$$\begin{aligned} \mathbf{X}(k+1) &= \mathbf{A}_1\mathbf{X}(k) + \mathbf{B}_0 u(k) + \mathbf{B}_2 u(k-2) \\ &\quad + \mathbf{B}_\tau u(k-1), \\ \mathbf{X}(k+2) &= \mathbf{A}_2\mathbf{X}(k+1) + \mathbf{B}_0 u(k+1) + \mathbf{B}_2 u(k-1) \\ &\quad + \mathbf{B}_\tau u(k-1), \\ &\vdots \\ \mathbf{X}(k+n) &= \mathbf{A}_n\mathbf{X}(k+n-1) + \mathbf{B}_0 u(k+n-1) + \mathbf{B}_2 u(k+n-3) \\ &\quad + \mathbf{B}_\tau u(k-1), \\ y(k) &= \mathbf{C}_\tau \mathbf{X}(k). \end{aligned} \tag{40}$$

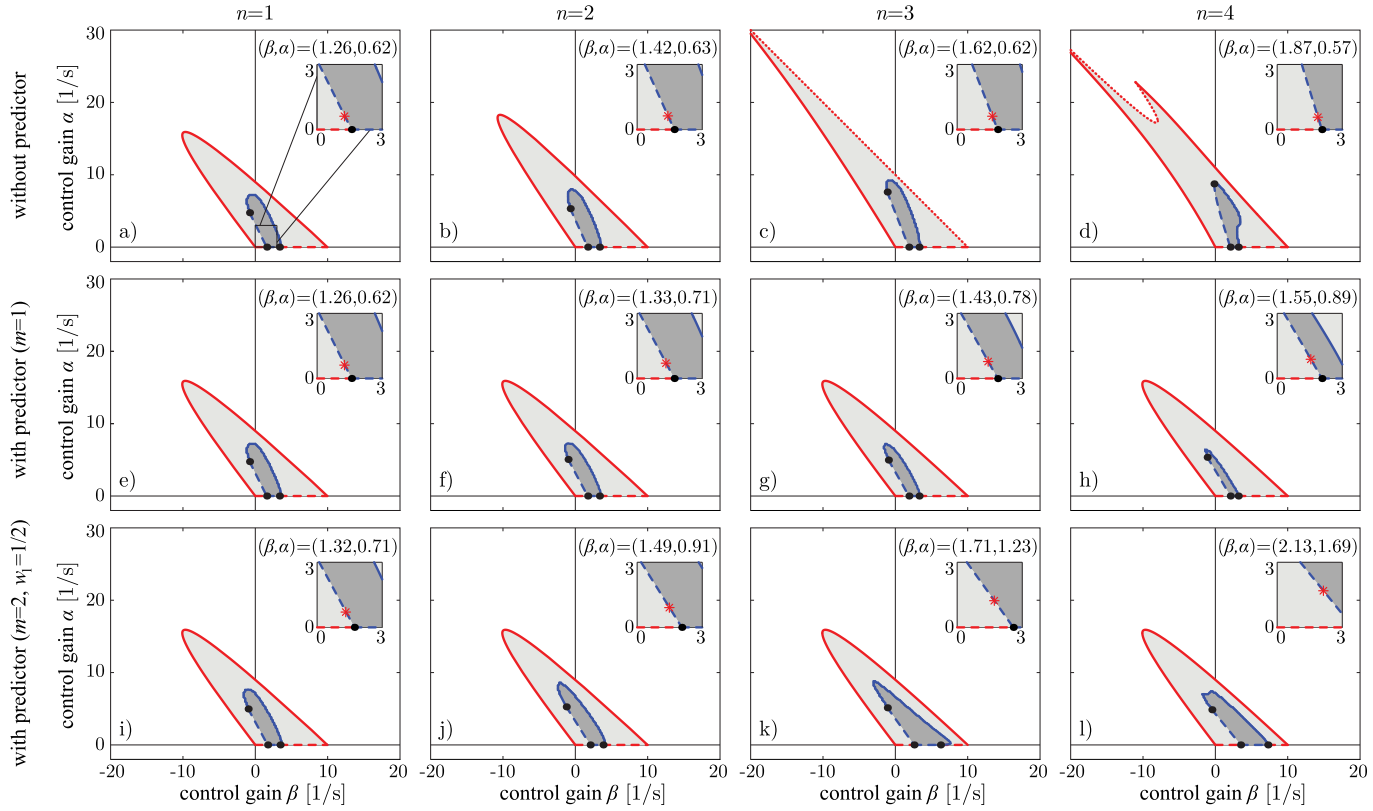

Fig. 5. Stability charts in the (β, α)-plane of the control gains for $\Delta t = 100$ [ms] when every n-th packet is received; (a-d) without predictor, (e-h) with predictor (45)-(46) using $m = 1$, (i-l) with predictor (45)-(46) using $m = 2$, $w_1 = 1/2$. The same color and shading scheme is used as in Fig. 4.

We analyze plant stability the same way as shown in Section IV. We substitute $u(k) = 0$ into (40) to obtain

$$\mathbf{X}(k+n) = \mathbf{A}\mathbf{X}(k), \tag{41}$$

where $\mathbf{A} = \prod_{j=1}^{n} \mathbf{A}_j$. The eigenvalues of $\mathbf{A}$ must be located within the unit circle of the complex plane to ensure plant stability. We calculate the plant stability boundaries analytically by solving the characteristic equation for the control gains given in the form of (22) while substituting $\mathbf{A}_1$ with $\mathbf{A}$ and assuming $z = 1$, $z = -1$, and $z = \mathrm{e}^{\mathrm{i}\theta}$.

We carry out the string stability analysis by applying Z-transform to (40) that yields the transfer function

$$\Gamma_n(z) = \mathbf{C}_\tau \left(z^n \mathbf{I} - \mathbf{A}\right)^{-1} \mathbf{G}_n(z), \tag{42}$$

where $\mathbf{G}_n(z)$ is given by the recursive rule

$$\begin{aligned} \mathbf{G}_1(z) &= \mathbf{B}_0 + \mathbf{B}_2 z^{-2} + \mathbf{B}_\tau z^{-1}, \\ \mathbf{G}_k(z) &= \mathbf{A}_k \mathbf{G}_{k-1}(z) + \mathbf{B}_0 z^{k-1} + \mathbf{B}_2 z^{k-3} + \mathbf{B}_\tau z^{-1}, \end{aligned} \tag{43}$$

for $k = 2, \ldots, n$. The $\omega_{\mathrm{cr}} = 0$ and the $\omega_{\mathrm{cr}} = (2k+1)\pi/\Delta t$ string stability boundaries can be calculated analytically the same way as discussed in Section IV. However, due to the algebraic complexity of the transfer function (42)-(43), the $0 < \omega_{\mathrm{cr}} \neq (2k+1)\pi/\Delta t$ string stability boundary cannot be obtained analytically. Instead, we create a grid in the (β, α)-plane, and we check in each point whether $\left|\Gamma_n\left(\mathrm{e}^{\mathrm{i}\omega\Delta t}\right)\right| < 1$ holds for $\omega \in (0, 2\pi/\Delta t)$.

The stability charts are presented in the (β, α)-plane for $n = 2, 3, 4$ in Fig. 5(b,c,d), where we used the same color and shading scheme as in Fig. 4(a). It is important to note that the controller cannot anticipate how frequent the packet losses will be. Therefore, the control parameters must be chosen such that the system is stable for any packet loss scenario (for any reasonable value of n). We can see that the stable domains vary significantly as n increases, therefore it is more difficult to find a pair of control gains that is stable for all packet loss scenarios. If n is increased further ($n > 4$), the dark grey shaded string stable region shrinks and disappears at $n = 10$.

TABLE I
DIMENSIONLESS CRITICAL SAMPLING PERIOD WHEN EVERY n-TH PACKET IS RECEIVED

$\Delta t_{\mathrm{cr}}/T_{\mathrm{h}}$	$n=1$	$n=2$	$n=3$	$n=4$
without predictor	0.333	0.286	0.247	0.215
predictor (45)-(46), $w_1 \to \infty$	0.5	0.333	0.25	0.2
predictor (62)	0.5	0.4	0.389	0.286
predictor (64), $w_1 \to \infty$	0.5	0.333	0.25	0.2

The size of the stable region depends on the sampling period as discussed in Section IV. Above a critical sampling period, $\Delta t > \Delta t_{\mathrm{cr}}$, the plant and string stable domain vanishes. For different packet loss scenarios, that is, for different values of n, the critical sampling period can be calculated by locating the intersection points of the string stability boundaries, and determining the sampling period where they coincide; see details of the $n = 1$ case in Appendix. The first row of Table I shows the critical sampling period for $n = 1, 2, 3, 4$, respectively. It is important to note that the more frequent the packet losses get,

the smaller the critical sampling period becomes. Hence frequent packet losses destabilize the system if the sampling time is not small enough. Note that the results in Table I also show that for a given Δt, the minimum achievable time gap $T_{\rm h} = 1/V'(h^*)$ between the vehicles increases as the packets are lost, that is, the maximum achievable flux in the traffic flow decreases.

In addition, it is important to note that large control gains imply large acceleration that the follower's engine may not be able to realize or may not be permitted in the presence of human passengers. When the controller gets into saturation, the linear stability analysis is not valid any more. The minimum gains that make the system string stable are shown in Fig. 5 by enlarging the stable region around the origin. The closest string stable points to the origin (where $\alpha^2+\beta^2$ is minimal) are also indicated by red stars on the inlets. Notice that the smallest available gains increase when packets are lost.

VI. Compensation of Packet Losses via Prediction

In this section, we propose a method to compensate for the destabilizing effects of the increasing time delay induced by packet losses. The method is based on the prediction of the leader's velocity and the headway data lost during communication. Accordingly, we use a predicted headway $h^{\rm P}$ and a predicted leader's velocity $v_{\rm L}^{\rm P}$ in the control law:

$$\begin{aligned} \dot v_{\rm F}(t) &= a_{\rm des}(t_{k-1}), \quad t \in [t_k, t_{k+1}), \\ a_{\rm des}(t_{k-1}) &= \alpha \left(V\big(h^{\rm P}(t_{k-1})\big) - v_{\rm F}(t_{k-1}) \right) \\ &\quad + \beta \left(W\big(v_{\rm L}^{\rm P}(t_{k-1})\big) - v_{\rm F}(t_{k-1}) \right), \end{aligned} \tag{44}$$

cf. (35).

To predict the leader's velocity we use earlier data. More precisely, we propose to compute the predicted leader's velocity as a weighted sum (average) of the last m available leader's velocity data:

$$v_{\rm L}^{\rm P}(t_{k-1}) = \sum_{i=1}^{m} w_i v_{\rm L}(t_{k-\tau_i(k)}), \tag{45}$$

where the weights are indicated by w_i and can be chosen when designing the predictor. The weights w_i must satisfy $\sum_{i=1}^m w_i = 1$ in order to preserve the equilibrium velocity of the uniform flow for the nonlinear system (1), (44). Parameter m denotes how many previously received data packets are used for computing the predicted leader's velocity – here we keep this fixed, independent of time. Parameters $\tau_i(k)$ indicate how many time steps earlier were the particular data packets received. For instance, if at t_k the last two leader's velocity data arrived 3 and 7 time steps ago, then $\tau_1(k) = 3$ and $\tau_2(k) = 7$, and using both of these in the prediction corresponds to $m = 2$. Note that the data packets may not be evenly distributed in time and any packet loss scenario can be described by $\tau_i(k)$. In the special case where every n-th packet is received and the last packet arrived $\tau(k)$ time steps earlier, $\tau_i(k) = \tau(k) + (i-1)n$, $i = 1, 2, \ldots, m$.

By definition, the headway is the difference of the distances traveled by the leader and the follower. We can predict this

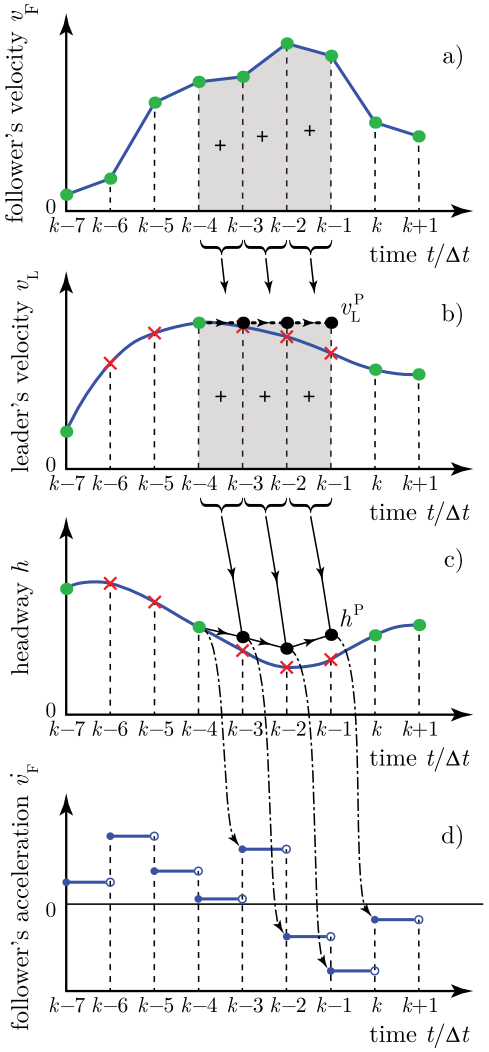

Fig. 6. Illustration of the prediction and the control processes with prediction algorithm (45)-(46) and control law (44) for $m = 1$, $w_1 = 1$, $\tau_1(k) = 4$. (a) (b) and (c) Green dots and red crosses show received and lost data packets, respectively, black dots show predicted data. Dashed arrows indicate the data used for leader's velocity prediction, whereas the shaded areas and the solid arrows show the data used for headway prediction. (d) Dashed-dotted arrows show which data is used by the controller to set the follower's acceleration.

by integrating (1). The key point is how we approximate the integrals of $v_{\rm L}(t)$ and $v_{\rm F}(t)$. Since the controller prescribes a piecewise constant acceleration for the follower, the velocity $v_{\rm F}(t)$ is piecewise linear. Hence, we predict the distance that the follower travels by approximating the area under $v_{\rm F}(t)$ by trapezoids; see Fig 6(a). Whereas we predict the distance that the leader travels by approximating the area under $v_{\rm L}(t)$ by a rectangle using the predicted velocity $v_{\rm L}^{\rm P}$; see Fig 6(b). The predicted headway becomes

$$\begin{aligned} h^{\rm P}(t_{k-1}) &= h(t_{k-\tau(k)}) + v_{\rm L}^{\rm P}(t_{k-1})(\tau(k)-1)\Delta t \\ &\quad - \sum_{j=1}^{\tau(k)-1} \frac{v_{\rm F}(t_{k-j-1}) + v_{\rm F}(t_{k-j})}{2} \Delta t, \end{aligned} \tag{46}$$

for $\tau(k) \geq 2$. For $\tau(k) = 1$, no packet is lost and we omit the sum in (46) to get $h^{\rm P}(t_{k-1}) = h(t_{k-1})$. Thus no headway prediction is done when a packet is received. Note, however, that the leader's velocity is predicted by (45) even

for $\tau(k) = 1$, so there is a possibility to improve string stability properties even when no packets are lost.

The method (45)-(46) to predict the leader's velocity and the headway is illustrated in Fig. 6 for the special case $m = 1$, $w_1 = 1$, $\tau_1(k) = 4$, that is, when the predictor relies on the data obtained 4 sampling periods earlier. Blue curves show the follower's velocity, the leader's velocity, the headway, and the follower's acceleration as a function of time. Green dots indicate when packets are received and red crosses stand for packet losses. In case of packet losses, the leader's velocity and the headway are predicted as shown by the black dots. The choice $m = 1$ yields that the leader's velocity is predicted to be the same as the last available data: $v_{\mathrm{L}}^{\mathrm{P}}(t_{k-1}) = v_{\mathrm{L}}(t_{k-\tau(k)})$, see the dashed arrows in Fig. 6(b). This way, the controller assumes that the leader's velocity does not change during packet losses, and the distance that the leader travels is computed accordingly. The headway is predicted by (46) by adding the difference of the distances that the leader and the follower travel during packet losses to the last available headway data; see the shaded areas and the solid arrows in Fig. 6(a,b,c). The dashed-dotted arrows in Fig. 6(d) show how the follower's acceleration is set according to the control law (44).

Another special case of predictor (45)-(46) is when $m = 2$, that is, the predictor uses the last two available leader's velocity values obtained $\tau_1(k)$ and $\tau_2(k)$ time instants earlier. Then, the leader's predicted velocity in Fig. 6(b) changes to $v_{\mathrm{L}}^{\mathrm{P}}(t_{k-1}) = w_1\ v_{\mathrm{L}}(t_{k-\tau_1(k)}) + w_2\ v_{\mathrm{L}}(t_{k-\tau_2(k)})$, where $w_2 = 1 - w_1$. If $w_1 = 1$ and $w_2 = 0$, we get back the case $m = 1$. If $w_1 = w_2 = 1/2$, the leader's velocity is predicted to be the average of the last two available leader's velocity data, and the headway predictor (46) uses this average velocity to calculate the distance that the leader travels during packet losses. It is also possible to predict the leader's velocity by linear extrapolation from the last two available data by choosing $w_1 = (\tau_2(k) - 1)/(\tau_2(k) - \tau_1(k))$ and $w_2 = 1 - w_1$. Note that the choice of m and w_i does not modify the prediction of the distance that the follower travels shown by the shaded area in Fig 6(a).

Now we solve (1), (44)-(46) with (12) along $[t_k, t_{k+1})$, and linearize the resulting discrete-time map, which yields

$$\mathbf{X}(k+1) = \mathbf{A}_{\tau(k)}^{\mathrm{P}}\mathbf{X}(k) + \mathbf{B}_0 u(k) + \mathbf{B}_2 u(k-2) + \sum_{i=1}^{m} w_i \mathbf{B}_{\tau(k)}^{\mathrm{P}} u\big(k - \tau_i(k)\big), \quad (47)$$

where

$$\mathbf{A}_{\tau(k)}^{\mathrm{P}} = \mathbf{A}_{\tau(k)} + \Delta\mathbf{A}_{\tau(k)}, \quad \mathbf{B}_{\tau(k)}^{\mathrm{P}} = \mathbf{B}_{\tau} + \Delta\mathbf{B}_{\tau(k)}, \quad (48)$$

and

$$\Delta\mathbf{A}_{\tau(k)} = \begin{bmatrix} \mathbf{0} & \mathbf{a}^{\mathrm{P}}/2 & \mathbf{a}^{\mathrm{P}} & \cdots & \mathbf{a}^{\mathrm{P}} & \mathbf{a}^{\mathrm{P}}/2 & \mathbf{0} & \cdots & \mathbf{0} & \mathbf{0} \\ \mathbf{I} & \mathbf{0} & \cdots & \mathbf{0} & \mathbf{0} & & & & & \\ \mathbf{0} & \mathbf{I} & & & \cdots & & & & \mathbf{0} & \mathbf{0} \\ \vdots & \vdots & & & \ddots & & & & \vdots & \vdots \\ \mathbf{0} & \mathbf{0} & & & \cdots & & & & \mathbf{I} & \mathbf{0} \end{bmatrix},$$

$$\Delta\mathbf{B}_{\tau(k)} = \begin{bmatrix} \mathbf{b}_{\tau(k)}^{\mathrm{P}} \\ \mathbf{o} \\ \vdots \\ \mathbf{o} \end{bmatrix}, \quad \mathbf{a}^{\mathrm{P}} = \begin{bmatrix} 0 & \frac{1}{2}\alpha V'(h^*)\Delta t^3 \\ 0 & -\alpha V'(h^*)\Delta t^2 \end{bmatrix},$$

$$\mathbf{b}_{\tau(k)}^{\mathrm{P}} = \begin{bmatrix} -\frac{1}{2}(\tau(k)-1)\alpha V'(h^*)\Delta t^3 \\ (\tau(k)-1)\alpha V'(h^*)\Delta t^2 \end{bmatrix}, \quad (49)$$

where there are $\tau(k)$ nonzero blocks in the first row of $\Delta\mathbf{A}_{\tau(k)}$, cf. (38), (39).

The stability analysis in the presence of the predictor can be done the same way as discussed in Section IV. The second and third rows of Fig. 5 show the stability diagrams using predictor (45)-(46) with $m = 1$ and with $m = 2$, $w_1 = 1/2$, respectively, for $n = 1, 2, 3, 4$. The color and shading scheme is the same as used in Fig. 4(a). We can assess the effect of predictor (45)-(46) by comparing the rows of Fig. 5. Based on the first row of Fig. 5, the plant stable domains vary significantly for the different packet loss scenarios when no predictor is used. In comparison, the second and third rows of Fig. 5 show that these domains remain exactly the same using predictor (45)-(46) as for no packet loss and no prediction, cf. Fig. 5(a). This implies that plant stability can be preserved by implementing predictors on the headway. The reason of the robustness of plant stability with respect to packet losses is the following. During plant stability analysis, we investigate stability in the absence of the leader's velocity fluctuations. Thus, only the headway needs to be predicted in order to improve plant stability. Since the follower's velocity is not affected by packet losses, it is available for the controller and can be integrated to obtain the exact headway for any packet loss scenario. This leads to the preservation of plant stability properties.

According to the first and second rows of Fig. 5, the choice $m = 1$ fails to increase the size of the string stable region. However, by choosing $m = 2$, the weight w_1 can be used as a design tool for enhancing string stability properties. Based on several case studies, the optimal choice of w_1 in terms of the size of the string stable region is around $w_1 = 1/2$; see the third row of Fig. 5. A heuristic argument supporting this choice is the following. When every n-th packet is delivered, the relation between $v_{\mathrm{L}}^{\mathrm{P}}(t_{k-1})$ and $v_{\mathrm{L}}(t_{k-\tau(k)})$ can be characterized by the transfer function $\Gamma^{\mathrm{P}}(z) = w_1 + w_2\, z^{-n}$ where $w_2 = 1 - w_1$. Consequently, prediction introduces a gain and a phase shift in the leader's velocity. The square of the gain is obtained as $\left|\Gamma^{\mathrm{P}}\left(\mathrm{e}^{\mathrm{i}\omega\Delta t}\right)\right|^2 = 1 - 4\, w_1(1-w_1)\sin^2(n\omega\Delta t/2)$, which is minimal for $w_1 = 1/2$. Indeed, we see improvements of string stability when applying the predictor with $m = 2$, $w_1 = 1/2$ in the third row of Fig. 5. The string stable regions become larger compared to the first row of Fig. 5, especially for frequent packet losses ($n = 3, 4$).

It is important to highlight that for $m = 2$, the weight $w_1 = 1/2$ is optimal in terms of the size of the stable region. This choice may not be optimal in terms of the minimal gains that make the system string stable. According to the second and third rows of Fig. 5, smaller gains can be achieved for $w_1 = 1$ (which gives case $m = 1$) than for $w_1 = 1/2$ as highlighted by the inlets. We can also analyze the effect of

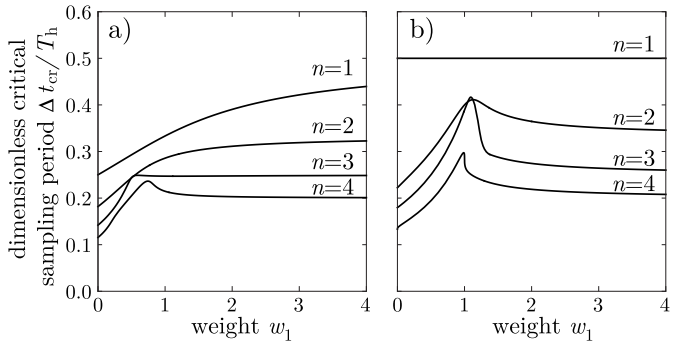

Fig. 7. The dimensionless critical sampling period $\Delta t_{\rm cr}/T_{\rm h}$ as a function of the weight w_1 used for prediction with $m = 2$ when every n-th packet is received (a) for predictor (45)-(46), (b) for the improved predictor (64).

prediction on the critical sampling period. Fig. 7(a) presents analytical results obtained by computer algebra for the dimensionless critical sampling period $\Delta t_{\rm cr}/T_{\rm h}$ as a function of the weight w_1. It can be seen that for $n = 1, 2$ the functions are monotonously increasing, whereas for $n = 3, 4$ the curves peak at $w_1 = 0.59$ and $w_1 = 0.74$, respectively. Based on Fig. 7, in order to increase the critical sampling period for any packet loss scenario (for all n), the best strategy is to choose w_1 as big as possible. The value of the dimensionless critical sampling period $\Delta t_{\rm cr}/T_{\rm h}$ converges to $1/(n+1)$ as $w_1 \to \infty$ as spelled out in the second row of Table I. For a given sampling period, we can achieve a smaller time gap between the vehicles and a larger flux in the traffic flow by choosing a large w_1.

Finally we remark that although string stability can be preserved for large sampling periods using a large weight w_1, the string stable region itself becomes very small. In such cases, the control parameters α and β must be set very accurately to realize stable control. Consequently, there is a trade-off when choosing the weight: $w_1 = 1/2$ gives larger stable region but with smaller critical sampling period, and $w_1 \to \infty$ gives large critical sampling period but small stable region. A similar trade-off was observed for a controller based on acceleration feedback proposed in [22]. Using that method it was possible to increase the critical time delay to infinity but with the cost that the size of the stable region becomes infinitely small.

VII. Compensation of the Processing Delay

In this section, we present another idea to improve plant and string stability properties in connected vehicle systems. First, we show this concept for the case where every data packet is received. Recall that using zero-order-hold introduces a time-periodic time delay in connected cruise control, cf. Fig. 3. The effective time delay is a saw-tooth function that increases from Δt in each period. Here, we call the delay Δt at the minima of the saw-tooth function as processing delay. Now we introduce an algorithm to compensate the processing delay introduced by the zero-order-hold.

The processing delay is caused by the fact that it takes a certain amount of time to process and transmit the sensed data and to receive the data, process it and use it for actuating the follower. Thus, at time t_k, only the control input $a_{\rm des}(t_{k-1})$ is available, which is calculated from the data measured at t_{k-1}. In other words, $a_{\rm des}(t_k)$ cannot be used in control law (8) due to the processing delay. On the other hand, since the control input applied along $[t_{k-1}, t_k)$ is known to the follower, it can be used to calculate the state at t_k provided that an accurate model about the motion of the vehicles is available. This way, the state is predicted one sampling period ahead in order to compensate the processing delay.

We propose the following predictor feedback control for the connected vehicle system:

$$\begin{aligned} \dot{v}_{\rm F}(t) &= a_{\rm des}(t_{k-1}), \quad t \in [t_k, t_{k+1}), \\ a_{\rm des}(t_{k-1}) &= \alpha \left(V\big(h^{\rm Q}(t_k)\big) - v_{\rm F}^{\rm Q}(t_k) \right) \\ &\quad + \beta \left(W\big(v_{\rm L}^{\rm Q}(t_k)\big) - v_{\rm F}^{\rm Q}(t_k) \right), \end{aligned} \tag{50}$$

cf. (35) and (44). As for the leader, we assume that its velocity does not change along $[t_{k-1}, t_k)$. We use the last available leader's velocity data as predicted value $v_{\rm L}^{\rm Q}(t_k)$, since the equation of motion is unknown for the leader and model-based prediction cannot be made. The follower's predicted velocity $v_{\rm F}^{\rm Q}(t_k)$ and the predicted headway $h^{\rm Q}(t_k)$ are obtained by assuming that over $[t_{k-1}, t_k)$ the follower indeed realizes the desired acceleration that is $a_{\rm des}(t_{k-2})$ according to (50). Integrating (1) and (50) over $[t_{k-1}, t_k)$ we get the predicted state as

$$\begin{aligned} v_{\rm F}^{\rm Q}(t_k) &= v_{\rm F}(t_{k-1}) + a_{\rm des}(t_{k-2})\Delta t, \\ v_{\rm L}^{\rm Q}(t_k) &= v_{\rm L}(t_{k-1}), \\ h^{\rm Q}(t_k) &= h(t_{k-1}) + \big(v_{\rm L}(t_{k-1}) - v_{\rm F}(t_{k-1})\big)\Delta t \\ &\quad - \frac{1}{2} a_{\rm des}(t_{k-2})\Delta t^2. \end{aligned} \tag{51}$$

Note that more detailed vehicle models such as the one in [23] could also be used instead of (50) for prediction.

Control law (50)-(51) can be considered as an application of the predictor feedback control technique called finite spectrum assignment (FSA) [1], which was developed for time delay compensation in feedback loops. Since here the control input is piecewise constant, the effective time delay cannot be completely compensated: it remains a time-varying saw-tooth function as in Fig. 3. However, using the control law (50)-(51) the saw-tooth can effectively be "pushed down" to zero for the follower's velocity using model-based prediction.

Similarly to the analysis in Section III, we derive a discrete-time map corresponding to (1), (50)-(51). First, we substitute the predicted headway and velocities in (51) into the control law (50). At this point, we can recognize that the desired acceleration $a_{\rm des}(t_{k-1})$ depends on its value $a_{\rm des}(t_{k-2})$ at the previous sampling instant. Therefore, we augment the state of the system by the follower's acceleration: $a_{\rm des}(k-1)$ becomes an element of the state vector.

Accordingly, after solving (1), (50)-(51) along $[t_k, t_{k+1})$, linearizing the resulting map, and substituting the sinusoidal fluctuations (12), we get

$$\begin{aligned} \mathbf{x}(k+1) &= \mathbf{a}_0\,\mathbf{x}(k) + \mathbf{b}_0\,u(k) + \mathbf{b}_1\,u(k) + \mathbf{b}_2\,u(k-2), \\ y(k) &= \mathbf{c}\,\mathbf{x}(k), \end{aligned} \tag{52}$$

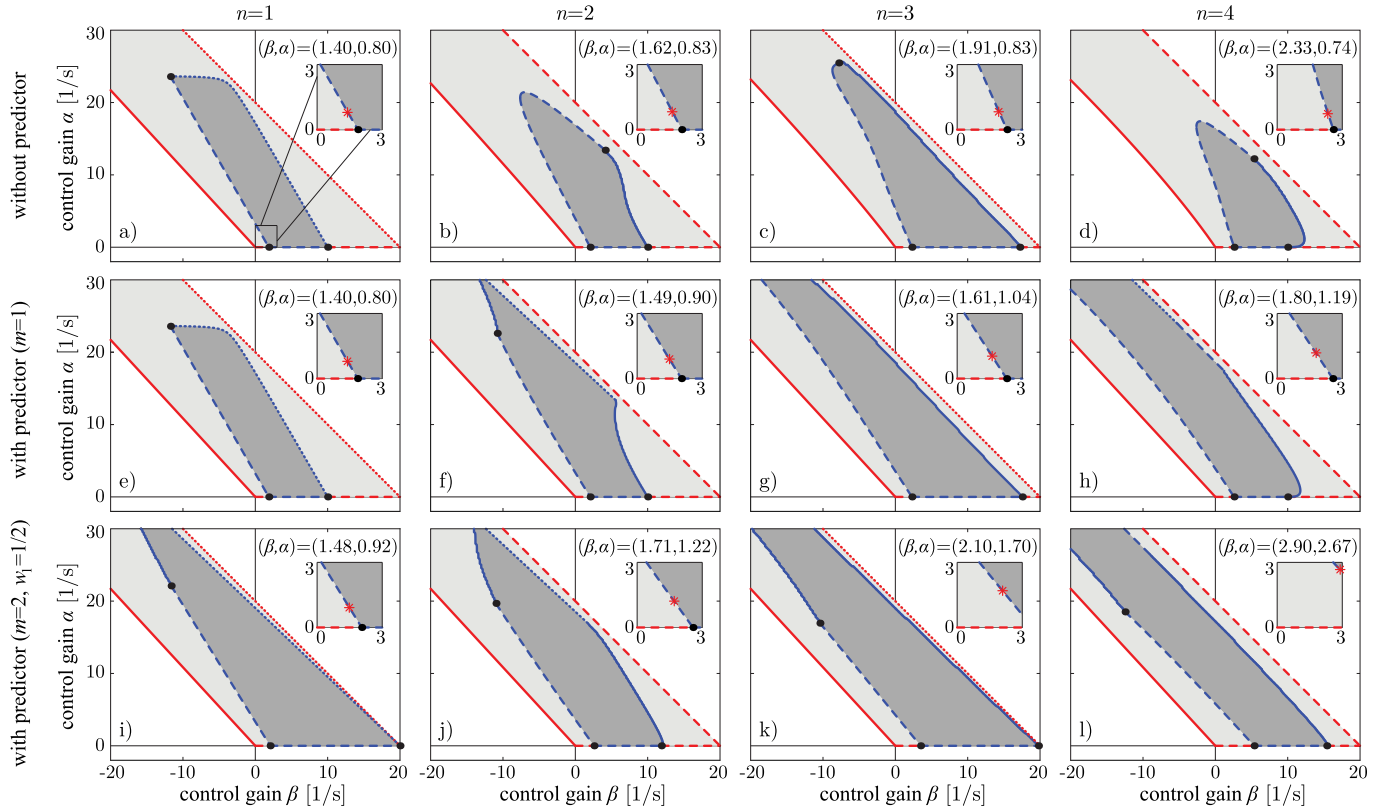

Fig. 8. Stability charts in the (β, α)-plane of the control gains for $\Delta t = 100$ [ms] when every n-th packet is received; (a-d) using controller (50)-(51), (e-h) using predictor (64) with $m = 1$, (i-l) using predictor (64) with $m = 2$, $w_1 = 1/2$. The same color and shading scheme is used as in Fig. 4.

where the state $\mathbf{x}(k)$, the input $u(k)$, and the output $y(k)$ are defined as

$$\mathbf{x}(k) = \begin{bmatrix} \tilde{h}(k) \\ \tilde{v}_{\mathrm{F}}(k) \\ \tilde{a}_{\mathrm{des}}(k-1) \end{bmatrix}, \quad u(k) = \tilde{v}_{\mathrm{L}}(k), \quad y(k) = \tilde{v}_{\mathrm{F}}(k), \tag{53}$$

and the coefficient matrices read

$$\begin{aligned} \mathbf{a}_0 &= \begin{bmatrix} 1 & -\Delta t & -\frac{1}{2}\Delta t^2 \\ 0 & 1 & \Delta t \\ \alpha V'(h^*) & a_{0,32} & a_{0,33} \end{bmatrix}, \\ a_{0,32} &= -\alpha V'(h^*)\Delta t - (\alpha + \beta), \\ a_{0,33} &= -\frac{1}{2}\alpha V'(h^*)\Delta t^2 - (\alpha + \beta)\Delta t, \\ \mathbf{b}_0 &= \begin{bmatrix} \beta_0 \\ 0 \\ 0 \end{bmatrix}, \quad \mathbf{b}_2 = \begin{bmatrix} \beta_2 \\ 0 \\ 0 \end{bmatrix}, \quad \mathbf{b}_1 = \begin{bmatrix} 0 \\ 0 \\ \beta + \alpha V'(h^*)\Delta t \end{bmatrix}, \\ \mathbf{c} &= \begin{bmatrix} 0 & 1 & 0 \end{bmatrix}, \end{aligned} \tag{54}$$

cf. (15)-(17). Note that in (52), $\mathbf{b}_1$ is the coefficient of $u(k)$ and not $u(k-1)$. This is due to the fact that the state was augmented by the desired acceleration a_{des}. Finally, the augmented state-space representation is obtained from (54) with $\mathbf{X}(k) = \mathbf{x}(k)$, $\mathbf{A}_1 = \mathbf{a}_0$, $\mathbf{B}_0 = \mathbf{b}_0$, $\mathbf{B}_1 = \mathbf{b}_1$, $\mathbf{B}_2 = \mathbf{b}_2$, $\mathbf{C}_1 = \mathbf{c}$ (cf. (18)-(20)).

The plant and the string stability of (52) can be analyzed following the steps of Section IV. The $z = 1$, the $z = -1$, and the $z = \mathrm{e}^{\mathrm{i}\theta}$, $\theta \in (0, \pi)$ plant stability boundaries are

$$\alpha = 0, \tag{55}$$

$$\alpha = \frac{2}{\Delta t} - \beta, \tag{56}$$

$$\alpha = \frac{-2\left(\cos(\theta) - 1\right)}{V'(h^*)\Delta t^2}, \quad \beta = \frac{\left(2 - V'(h^*)\Delta t\right)\left(\cos(\theta) - 1\right)}{V'(h^*)\Delta t^2}, \tag{57}$$

respectively. The $\omega_{\mathrm{cr}} = 0$ string stability boundaries read

$$\alpha = 0, \tag{58}$$

$$\alpha = \frac{2\left(V'(h^*) - \beta + \beta V'(h^*)\Delta t\right)}{1 - 7\left(V'(h^*)\right)^2 \Delta t^2/6}, \tag{59}$$

whereas for $\omega_{\mathrm{cr}} = (2k+1)\pi/\Delta t$ we get

$$\beta = \frac{\left(\pi^2 - (\pi^2+1)V'(h^*)^2\Delta t^2\right)\Delta t^2\alpha^2 - 4\pi^2\Delta t\alpha + 4\pi^2}{2\pi^2\Delta t\left(\left(V'(h^*)\Delta t - 1\right)\Delta t\alpha + 2\right)}. \tag{60}$$

The $0 < \omega_{\mathrm{cr}} \neq (2k+1)\pi/\Delta t$ string stability boundaries are given in the form of (32). These can only be obtained numerically and they are not physically relevant in this case.

Fig. 8(a) presents the stability chart of the system with processing delay compensation in the absence of packet loss. The color and shading scheme is the same as in Fig. 4. In comparison to Fig. 5(a), improvement can be observed both in terms of plant and string stability owing to the processing delay compensation.

The value of the critical sampling period, above which string stability cannot be guaranteed, can be obtained in closed form using the same method as in Section IV and Appendix:

$$\Delta t_{\rm cr} = \frac{1}{2V'(h^*)}. \tag{61}$$

Comparing this to (33), we can see that the critical sampling period improves significantly, as it becomes 1.5 times larger compared to the case where a zero-order-hold is used without processing delay compensation. Therefore, the control loop remains stable for smaller time gap ($T_{\rm h} = 1/V'(h^*)$) between the vehicles for a given sampling period.

We expect that the better stability properties are beneficial even in the case of packet losses. In this case, the predictor can rely only on the leader's velocity and the headway of the last available packet. For $\tau(k)-1$ consecutive packet losses, the predictor becomes

$$\begin{aligned} v_{\rm F}^{\rm Q}(t_k) &= v_{\rm F}(t_{k-1}) + a_{\rm des}(t_{k-2})\Delta t,\\ v_{\rm L}^{\rm Q}(t_k) &= v_{\rm L}(t_{k-\tau(k)}),\\ h^{\rm Q}(t_k) &= h(t_{k-\tau(k)}) + \big(v_{\rm L}(t_{k-\tau(k)}) - v_{\rm F}(t_{k-1})\big)\Delta t\\ &\quad - \frac{1}{2}a_{\rm des}(t_{k-2})\Delta t^2, \end{aligned} \tag{62}$$

cf. (51).

Now we solve system (1), (50), (62) over $[t_k, t_{k+1})$, linearize the resulting nonlinear discrete-time map, and assume sinusoidal fluctuations (12) in the leader's velocity. We get the linear discrete-time map of the form (38)-(39) with slight modifications: $u\big(k-\tau(k)\big)$ is replaced by $u\big(k-\tau(k)+1\big)$, and the last block of the state vector becomes $\mathbf{x}\big(k-n+1\big)$ instead of $\mathbf{x}\big(k-n\big)$. The nonzero blocks in the first row of $\mathbf{A}_{\tau(k)}$ are

$$\tilde{\mathbf{a}}_0 = \begin{bmatrix} 1 & -\Delta t & -\frac{1}{2}\Delta t^2\\ 0 & 1 & \Delta t\\ 0 & a_{0,32} & a_{0,33}\end{bmatrix}, \quad \tilde{\mathbf{a}}_\tau = \begin{bmatrix} 0 & 0 & 0\\ 0 & 0 & 0\\ \alpha V'(h^*) & 0 & 0\end{bmatrix},$$
$$\begin{aligned} \tilde{a}_{0,32} &= -\alpha V'(h^*)\Delta t - (\alpha+\beta),\\ \tilde{a}_{0,33} &= -\frac{1}{2}\alpha V'(h^*)\Delta t^2 - (\alpha+\beta)\Delta t, \end{aligned} \tag{63}$$

where $\tilde{\mathbf{a}}_\tau$ is located in the $\tau(k)$-th column of $\mathbf{A}_{\tau(k)}$. Note that $\tilde{\mathbf{a}}_0 + \tilde{\mathbf{a}}_\tau = \mathbf{a}_0$, cf. (54) and (63). Matrices $\mathbf{b}_0$, $\mathbf{b}_2$, and $\mathbf{b}_\tau = \mathbf{b}_1$ are given by (54).

The stability diagrams and the critical sampling period can be determined by the method explained in Section IV. Fig. 8(b,c,d) present the stability charts of the system with processing delay compensation if every n-th packet is received, $n = 2, 3, 4$. Notice the improvement in plant and string stability compared to Fig. 5(b,c,d) – the proposed predictor feedback concept is robust against the variations of time delay caused by packet losses. The third row of Table I shows the values of the critical sampling period for $n = 1, 2, 3, 4$. These values are 1.5, 1.4, 1.58, 1.33 times larger, respectively, than those corresponding to the case without processing delay compensation. Thus, the critical sampling period improves even under the variations of time delay due to packet losses, and smaller time gap can be achieved between the vehicles for a given sampling period. Note, however, that there is an increase in the smallest gains that ensure string stability (indicated by the red stars) compared to the case without processing delay compensation, cf. Fig. 5.

Finally, the two predictive control strategies in Sections VI and VII can be combined to compensate both the effect of processing delay and the effect of packet losses. We use the control law (50) with the prediction algorithm

$$\begin{aligned} v_{\rm F}^{\rm Q}(t_k) &= v_{\rm F}(t_{k-1}) + a_{\rm des}(t_{k-2})\Delta t,\\ v_{\rm L}^{\rm Q}(t_k) &= v_{\rm L}^{\rm P}(t_{k-1}),\\ h^{\rm Q}(t_k) &= h^{\rm P}(t_{k-1}) + \big(v_{\rm L}^{\rm P}(t_{k-1}) - v_{\rm F}(t_{k-1})\big)\Delta t\\ &\quad - \frac{1}{2}a_{\rm des}(t_{k-2})\Delta t^2,\\ v_{\rm L}^{\rm P}(t_{k-1}) &= \sum_{i=1}^{m} w_i v_{\rm L}(t_{k-\tau_i(k)}),\\ h^{\rm P}(t_{k-1}) &= h(t_{k-\tau(k)}) + v_{\rm L}^{\rm P}(t_{k-1})(\tau(k)-1)\Delta t\\ &\quad - \sum_{j=1}^{\tau(k)-1} \frac{v_{\rm F}(t_{k-j-1}) + v_{\rm F}(t_{k-j})}{2}\Delta t, \end{aligned} \tag{64}$$

cf. (45)-(46), (51), and (62). That is, now the leader's velocity is predicted ($v_{\rm L}^{\rm P}(t_{k-1})$), the headway is corrected according to the difference of distances the two vehicles travel during the packet losses ($h^{\rm P}(t_{k-1})$), and also the follower's velocity and headway are predicted one sampling period ahead to compensate the processing delay ($v_{\rm F}^{\rm Q}(t_k), h^{\rm Q}(t_k)$).

Solving (1), (50), (64) over $[t_k, t_{k+1})$, linearizing the resulting map, and assuming sinusoidal fluctuations (12) in the leader's velocity yields the form (47)-(49) where $u\big(k-\tau_i(k)\big)$ is replaced by $u\big(k-\tau_i(k)+1\big)$, the nonzero blocks in the first row of $\Delta\mathbf{A}_{\tau(k)}$ are shifted to the first $\tau(k)$ columns, and

$$\mathbf{a}^{\rm P} = \begin{bmatrix} 0 & 0 & 0\\ 0 & 0 & 0\\ 0 & -\alpha V'(h^*)\Delta t & 0\end{bmatrix},$$
$$\mathbf{b}_{\tau(k)}^{\rm P} = \begin{bmatrix} 0\\ 0\\ \alpha V'(h^*)(\tau(k)-1)\Delta t\end{bmatrix}. \tag{65}$$

Analyzing plant and string stability according to Section IV, we obtain the stability charts shown in Fig. 8(e-l) if every n-th packet is received ($n = 1, 2, 3, 4$). Again we chose $m = 1$ and $m = 2$, $w_1 = 1/2$ in the second and the third rows, respectively. Comparing the results to those in Fig. 5 and Fig. 8(a-d), we can see that both predictive control strategies – headway and leader's velocity prediction as well as compensation of the processing delay – make improvements in stability, even when these are applied together. The weight $w_1 \approx 1/2$ is still an optimal choice in terms of the size of the stable region. It is still true that string stability can be guaranteed by smaller gains for $m = 1$ than for $m = 2$, $w_1 = 1/2$, see the red stars in Fig. 8(e-h) and Fig. 8(i-l). Again, processing delay compensation increases the smallest available control gains, cf. Fig. 5.

The dimensionless critical sampling period $\Delta t_{\rm cr}/T_{\rm h}$ as a function of the weight w_1 is depicted in Fig. 7(b) for the improved predictor presented in this Section. Based on the figure, the critical sampling period peaks around $w_1 \approx 1$. Therefore, in order to increase the critical sampling period

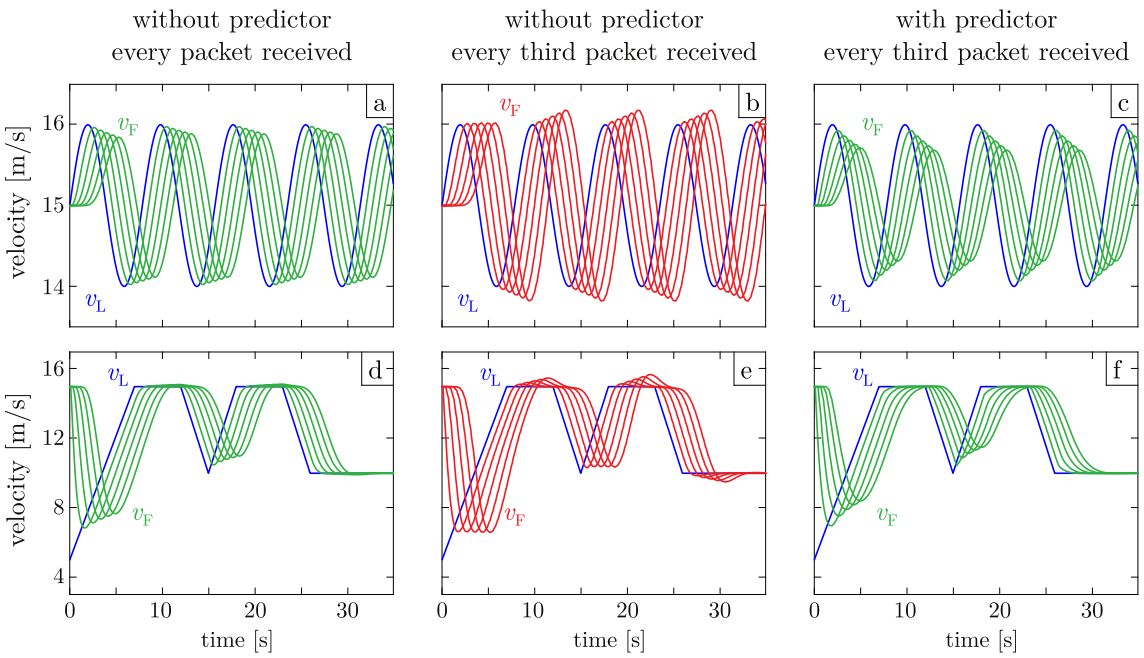

Fig. 9. Velocity response of a vehicle string with five followers (a,d) without predictor when every data packet is received ($n = 1$), (b,e) without predictor when every third packet is received ($n = 3$), (c,f) using predictor (64) with $m = 2$, $w_1 = 2$ when every third packet is received ($n = 3$). The first row (a-c) shows the response to sinusoidal leader's velocity fluctuations, the second row (d-f) presents the response in the case of a real traffic scenario.

for any n, or to increase the flux of the traffic flow for a given Δt, the best choice is $w_1 = 1$, that is, simply using the last available leader's velocity as predicted value. The value of the dimensionless critical sampling period $\Delta t_{\rm cr}/T_{\rm h}$ again converges to $1/(n+1)$ as $w_1 \to \infty$. Therefore, we get the same critical sampling period for $w_1 \to \infty$ as without processing delay compensation, cf. the fourth row of Table I. Predicting the leader's velocity is beneficial in terms of the size of the stable region, but only at the cost of the critical sampling period. In summary, there is trade-off between the size of the stable region, the critical sampling period, and the minimum gains that ensure string stability when we choose between the predictive control strategies (45)-(46), (51), and (64) and when we select the parameters of the predictor.

Finally, the performance of the predictor is demonstrated in Fig. 9 via numerical simulations of the nonlinear system (50), (64). The first row of Fig. 9 shows the response of five follower vehicles (the concatenation of five identical leader-follower pairs with simultaneous packet losses) to sinusoidal fluctuations in the leader's velocity assuming sampling period $\Delta t = 100$ [ms] and control gains $\alpha = 1.2$ [1/s], $\beta = 1$ [1/s]. This corresponds to a string stable scenario when no data packets are lost ($n = 1$), see Fig. 9(a). According to Fig. 9(b), the system becomes string unstable when packets are lost (when every third packet is received, $n = 3$). The application of predictor (64) with $m = 2$, $w_1 = 2$ makes the system string stable again as shown by Fig. 9(c). The second row of Fig. 9 shows the velocity response with the same control gains for a real traffic scenario where large fluctuations occur in the leader's velocity. It is again shown that string stability may be lost due to packet losses, but predictors can overcome this problem even in the case of large leader velocity perturbations.

VIII. Conclusions

In this paper, we analyzed a communication-based control strategy called connected cruise control (CCC) for vehicular strings. We have shown that the application of digital controllers introduces time-varying time delays in the control loop. The communication between the vehicles is often influenced by the loss of data packets, which increases the time delay. We analyzed the effect of the increasing time delay on the plant and the string stability of a connected vehicular string, and we have shown that packet losses have destabilizing effects. Namely, string stability cannot be achieved above a certain critical value of the sampling period or, equivalently, there exist a minimal achievable time gap between the vehicles for a given sampling period. This puts a fundamental limit to the achievable flux in the traffic flow of the connected vehicles.

Therefore, we proposed a method to overcome the destabilizing effect of packet losses using data received earlier. We demonstrated that predicting the leader's velocity and the headway, plant and string stability can be improved. Furthermore, we presented a predictor to compensate the processing delay of the digital controller. These modifications led to further improvements in the stability properties. Combining the two above-mentioned strategies, the critical sampling period of the controller and the maximum achievable flux could be increased by a large extent, and the connected cruise control became robust against the loss of data packets during communication.

We remark that during the processing delay compensation the model used for predicting the follower's motion is assumed to be accurate and that the desired acceleration is realized by the follower. Analyzing the effect of modeling uncertainties and inaccuracies in the implementation of the control law is left for future research. Moreover, we kept the form of the

controller as simple as possible and assumed simple packet loss scenarios in order to highlight the potential of predictors. Considering more detailed dynamical models of the vehicles, investigating more complicated control strategies, and taking into account stochastic packet loss scenarios are left for future work.

APPENDIX
DERIVATION OF THE CRITICAL SAMPLING PERIOD

Using (17), (20), and (26), the magnitude ratio (27) can be expressed by

$$M(\omega) = \frac{\mathrm{N}(\omega)}{\mathrm{D}(\omega)}, \tag{66}$$

where

$$\begin{aligned}\mathrm{N}^2(\omega) &= 4\big(\hat{V}^2\hat{\alpha}^2 + \hat{\omega}^2\hat{\beta}^2\big)\big(1-\cos\hat{\omega}\big),\\ \mathrm{D}^2(\omega) &= \Big(10 + \big(1+\hat{V}\hat{\alpha}\big)^2 + \big(1+2(\hat{\alpha}+\hat{\beta})\big)^2\Big)\hat{\omega}^2\\ &\quad - \Big(8 - \big(1-\hat{V}\hat{\alpha}\big)^2 + \big(3+2(\hat{\alpha}+\hat{\beta})\big)^2\Big)\hat{\omega}^2\cos\hat{\omega}\\ &\quad + \big(4 - 2\hat{V}\hat{\alpha} + 12(\hat{\alpha}+\hat{\beta})\big)\hat{\omega}^2\cos\big(2\hat{\omega}\big)\\ &\quad - \big(-2\hat{V}\hat{\alpha} + 4(\hat{\alpha}+\hat{\beta})\big)\hat{\omega}^2\cos\big(3\hat{\omega}\big),\end{aligned} \tag{67}$$

with $\hat{\alpha} = \alpha\Delta t$, $\hat{\beta} = \beta\Delta t$, $\hat{\omega} = \omega\Delta t$, and $\hat{V} = V'(h^*)\Delta t$. This allows us to obtain the string stability boundaries (29)-(32).

In Fig. 4(a), the intersection of (29) and (30) is marked by I, the intersection of (29) and (32) is marked by II, while the intersection of (30) and (32) is marked by III. Here we show that I, II, III coincide at the critical sampling time given by (33). From (29)-(30), the intersection I of the two $\omega_{\mathrm{cr}} = 0$ string stability boundaries is at $(\beta, \alpha) = (V'(h^*), 0)$. In the case of the other two intersection points II and III, a string stability boundary associated with $0 < \omega_{\mathrm{cr}} \neq (2k+1)\pi/\Delta t$ emanates from a $\omega_{\mathrm{cr}} = 0$ boundary. Therefore, we can find the two points in question by taking $\omega_{\mathrm{cr}} \to 0$ for the boundary defined by (32). However, conditions $M(0) = 1$ and $M'(0) = 0$ are not sufficient to find the two branch-off points, since they hold for any β and α. Besides, each point of the $\omega_{\mathrm{cr}} = 0$ string stability boundaries satisfies $M''(0) = 0$. Thus, the intersection points II and III satisfy $M'''(0) = 0$. Introducing

$$Q(\omega) = \mathrm{N}^2(\omega) - \mathrm{D}^2(\omega), \tag{68}$$

conditions $M''(0) = 0$ and $M'''(0) = 0$ are equivalent to $Q^{(4)}(0) = 0$ and $Q^{(6)}(0) = 0$, which can be solved more conveniently. Since $\alpha = 0$ is a solution of $Q^{(4)}(0) = 0$, cf. (29), we can determine the intersection point II by solving $Q^{(6)}(0)\big|_{\alpha=0} = 0$, which gives $\beta = 1/(3\Delta t)$. The points $(V'(h^*), 0)$ and $(1/(3\Delta t), 0)$ coincide for the critical sampling period given by (33). It can be shown that the branch-off point III defined by $Q^{(4)}(0) = 0$ and $Q^{(6)}(0) = 0$ also coincides with these two points when (33) holds.

REFERENCES

[1] M. Krstic, *Delay Compensation for Nonlinear, Adaptive, and PDE Systems*. Boston, MA, USA: Birkhäuser, 2009.

[2] A. Z. Manitius and A. W. Olbrot, "Finite spectrum assignment problem for systems with delays," *IEEE Trans. Autom. Control*, vol. AC-24, no. 4, pp. 541–552, Aug. 1979.

[3] Q.-G. Wang, T. H. Lee, and K. K. Tan, *Finite-Spectrum Assignment for Time-Delay Systems*. London, U.K.: Springer, 1999.

[4] W. Michiels and S.-I. Niculescu, *Stability and Stabilization of Time-Delay Systems—An Eigenvalue-Based Approach*. Philadelphia, PA, USA: SIAM, 2007.

[5] M. Jankovic, "Forwarding, backstepping, and finite spectrum assignment for time delay systems," *Automatica*, vol. 45, no. 1, pp. 2–9, 2009.

[6] D. Kleinman, "Optimal control of linear systems with time-delay and observation noise," *IEEE Trans. Autom. Control*, vol. AC-14, no. 5, pp. 524–527, Oct. 1969.

[7] K. Engelborghs, M. Dambrine, and D. Roose, "Limitations of a class of stabilization methods for delay systems," *IEEE Trans. Autom. Control*, vol. 46, no. 2, pp. 336–339, Feb. 2001.

[8] S. Mondié, M. Dambrine, and O. Santos, "Approximation of control laws with distributed delays: A necessary condition for stability," *Kybernetika*, vol. 38, no. 5, pp. 541–551, 2002.

[9] W. Michiels, S. Mondié, and D. Roose, "Robust stabilization of time-delay systems with distributed delay control laws: Necessary and sufficient conditions for a safe implementation," Dept. Comput. Sci., Katholieke Univ. Leuven, Leuven, Belgium, Tech. Rep. TW363, 2003.

[10] S. Mondié and W. Michiels, "Finite spectrum assignment of unstable time-delay systems with a safe implementation," *IEEE Trans. Autom. Control*, vol. 48, no. 12, pp. 2207–2212, Dec. 2003.

[11] T. G. Molnár and T. Insperger, "On the robust stabilizability of unstable systems with feedback delay by finite spectrum assignment," *J. Vibrat. Control*, vol. 22, no. 3, pp. 649–661, 2016.

[12] D. Schrank, B. Eisele, and T. Lomax, "Annual urban mobility report," Texas Transp. Inst., Texas A&M Univ. Syst., College Station, TX, USA, Tech. Rep. 70, 2012.

[13] D. Swaroop and J. K. Hedrick, "String stability of interconnected systems," *IEEE Trans. Autom. Control*, vol. 41, no. 3, pp. 349–357, Mar. 1996.

[14] G. Orosz, R. E. Wilson, R. Szalai, and G. Stépán, "Exciting traffic jams: Nonlinear phenomena behind traffic jam formation on highways," *Phys. Rev. E, Stat. Phys. Plasmas Fluids Relat. Interdiscip. Top.*, vol. 80, no. 4, p. 046205, 2009.

[15] G. Orosz, R. E. Wilson, and G. Stépán, "Traffic jams: Dynamics and control," *Philos. Trans. Roy. Soc. A, Math., Phys., Eng. Sci.*, vol. 368, no. 1928, pp. 4455–4479, 2010.

[16] A. Vahidi and A. Eskandarian, "Research advances in intelligent collision avoidance and adaptive cruise control," *IEEE Trans. Intell. Transp. Syst.*, vol. 4, no. 3, pp. 143–153, Sep. 2003.

[17] D. Caveney, "Cooperative vehicular safety applications," *IEEE Control Syst. Mag.*, vol. 30, no. 4, pp. 38–53, Aug. 2010.

[18] L. Zhang and G. Orosz, "Motif-based design for connected vehicle systems in presence of heterogeneous connectivity structures and time delays," *IEEE Trans. Intell. Transp. Syst.*, vol. 17, no. 6, pp. 1638–1651, Jun. 2016.

[19] R. Rajamani and S. E. Shladover, "An experimental comparative study of autonomous and co-operative vehicle-follower control systems," *Transp. Res. C, Emerg. Technol.*, vol. 9, no. 1, pp. 15–31, 2001.

[20] B. van Arem, C. J. G. van Driel, and R. Visser, "The impact of cooperative adaptive cruise control on traffic-flow characteristics," *IEEE Trans. Intell. Transp. Syst.*, vol. 7, no. 4, pp. 429–436, Dec. 2006.

[21] S. Öncü, J. Ploeg, N. van de Wouw, and H. Nijmeijer, "Cooperative adaptive cruise control: Network-aware analysis of string stability," *IEEE Trans. Intell. Transp. Syst.*, vol. 15, no. 4, pp. 1527–1537, Aug. 2014.

[22] J. I. Ge and G. Orosz, "Dynamics of connected vehicle systems with delayed acceleration feedback," *Transp. Res. C, Emerg. Technol.*, vol. 46, pp. 46–64, Sep. 2014.

[23] G. Orosz, "Connected cruise control: Modelling, delay effects, and nonlinear behaviour," *Vehicle Syst. Dyn.*, vol. 54, no. 8, pp. 1147–1176, 2016.

[24] J. B. Kenney, "Dedicated short-range communications (DSRC) standards in the United States," *Proc. IEEE*, vol. 99, no. 7, pp. 1162–1182, Jul. 2011.

[25] F. Pistorius, A. Lauber, J. Pfau, A. Klimm, and J. Becker, "Development of a latency optimized communication device for WAVE and SAE based V2X-applications," SAE Tech. Paper 2016-01-0150, Apr. 2016.

[26] *Dedicated Short Range Communications (DSRC) Message Set Dictionary Set*, SAE International Standard J2735SET_201603, 2016.

[27] W. B. Qin and G. Orosz, "Digital effects and delays in connected vehicles: Linear stability and simulations," in *Proc. ASME Dyn. Syst. Control Conf.*, 2013, p. V002T30A001, paper DSCC2013-3830.

[28] W. B. Qin, M. M. Gomez, and G. Orosz, "Stability and frequency response under stochastic communication delays with applications to connected cruise control design," *IEEE Trans. Intell. Transp. Syst.*, vol. 18, no. 2, pp. 388–403, Feb. 2017.

[29] L. C. Davis, "Stability of adaptive cruise control systems taking account of vehicle response time and delay," *Phys. Lett. A*, vol. 376, nos. 40–41, pp. 2658–2662, 2012.
[30] J. Ploeg, D. P. Shukla, N. van de Wouw, and H. Nijmeijer, "Controller synthesis for string stability of vehicle platoons," *IEEE Trans. Intell. Transp. Syst.*, vol. 15, no. 2, pp. 854–865, Apr. 2014.
[31] J. Ploeg, N. van de Wouw, and H. Nijmeijer, "$\mathcal{L}_p$ string stability of cascaded systems: Application to vehicle platooning," *IEEE Trans. Control Syst. Technol.*, vol. 22, no. 2, pp. 786–793, Mar. 2014.
[32] M. di Bernardo, A. Salvi, and S. Santini, "Distributed consensus strategy for platooning of vehicles in the presence of time-varying heterogeneous communication delays," *IEEE Trans. Intell. Transp. Syst.*, vol. 16, no. 1, pp. 102–112, Feb. 2015.
[33] V. Van Assche, M. Dambrine, J.-F. Lafay, and J.-P. Richard, "Implementation of a distributed control law for a class of systems with delay," in *Proc. 3rd IFAC Workshop Time Delay Syst.*, Santa Fe, NM, USA, 2001, pp. 266–271.
[34] G. F. Newell, "A simplified car-following theory: A lower order model," *Transp. Res. B, Methodol.*, vol. 36, no. 3, pp. 195–205, 2002.
[35] M. Wang, "Generic model predictive control framework for advanced driver assistance systems," Ph.D. dissertation, Dept. Transp. Planning, Delft Univ. Technol., Delft, The Netherlands, 2014.
[36] J. Ploeg, N. van de Wouw, and H. Nijmeijer, "Fault tolerance of cooperative vehicle platoons subject to communication delay," in *Proc. 12th IFAC Workshop Time Delay Syst.*, Ann Arbor, MI, USA, 2015, pp. 352–357.
[37] F. Gao, S. E. Li, Y. Zheng, and D. Kum, "Robust control of heterogeneous vehicular platoon with uncertain dynamics and communication delay," *IET Intell. Transport Syst.*, vol. 10, no. 7, pp. 503–513, 2016.
[38] J. I. Ge and G. Orosz, "Optimal control of connected vehicle systems with communication delay and driver reaction time," *IEEE Trans. Intell. Transp. Syst.*, vol. 18, no. 8, pp. 2056–2070, Aug. 2017.
[39] M. Wang, W. Daamen, S. P. Hoogendoorn, and B. van Arem, "Cooperative car-following control: Distributed algorithm and impact on moving jam features," *IEEE Trans. Intell. Transp. Syst.*, vol. 17, no. 5, pp. 1459–1471, May 2016.
[40] M. Wang, S. P. Hoogendoorn, W. Daamen, B. van Arem, B. Shyrokau, and R. Happee, "Delay-compensating strategy to enhance string stability of adaptive cruise controlled vehicles," *Transportmetrica B, Transport Dyn.*, to be published. [Online]. Available: http://dx.doi.org/10.1080/21680566.2016.1266973.
[41] Y. Zheng, S. E. Li, J. Wang, D. Cao, and K. Li, "Stability and scalability of homogeneous vehicular platoon: Study on the influence of information flow topologies," *IEEE Trans. Intell. Transp. Syst.*, vol. 17, no. 1, pp. 14–26, Jan. 2016.
[42] Y. Zheng, S. E. Li, K. Li, and L.-Y. Wang, "Stability margin improvement of vehicular platoon considering undirected topology and asymmetric control," *IEEE Trans. Intell. Transp. Syst.*, vol. 24, no. 4, pp. 1253–1265, Jul. 2016.
[43] C. R. He and G. Orosz, "Saving fuel using wireless vehicle-to-vehicle communication," in *Proc. Amer. Control Conf.*, 2017, pp. 4946–4951.
[44] V. Turri, B. Besselink, and K. H. Johansson, "Cooperative look-ahead control for fuel-efficient and safe heavy-duty vehicle platooning," *IEEE Trans. Control Syst. Technol.*, vol. 25, no. 1, pp. 12–28, Jan. 2017.
[45] B. Besselink *et al.*, "Cyber–physical control of road freight transport," in *Proc. IEEE*, vol. 104, no. 5, pp. 1128–1141, May 2016.
[46] K.-Y. Liang *et al.*, "Networked control challenges in collaborative road freight transport," *Eur. J. Control*, vol. 30, pp. 2–14, Jul. 2016.
[47] G. Stépán, "Vibrations of machines subjected to digital force control," *Int. J. Solids Struct.*, vol. 38, nos. 10–13, pp. 2149–2159, 2001.
[48] M. M. Gomez, W. B. Qin, G. Orosz, and R. M. Murray, "Exact stability analysis of discrete-time linear systems with stochastic delays," in *Proc. Amer. Control Conf.*, 2014, pp. 5534–5539.
[49] T. Insperger and G. Stépán, *Semi-Discretization for Time-Delay Systems—Stability and Engineering Applications*. New York, NY, USA: Springer, 2011.

Tamás G. Molnár received the M.Sc. degree in mechanical engineering from the Budapest University of Technology and Economics, Budapest, Hungary, in 2015, where he is currently pursuing the Ph.D. degree with the Department of Applied Mechanics.

His current research interests include time delay systems and nonlinear dynamics and control.

Wubing B. Qin received the B.Eng. degree from the Huazhong University of Science and Technology, Wuhan, China, in 2011. He is currently pursuing the Ph.D. degree in mechanical engineering with the University of Michigan, Ann Arbor, MI, USA.

His current research interests include the dynamics and control of connected vehicles and nonlinear and stochastic systems with time delays.

Tamás Insperger received the M.Sc. and Ph.D. degrees in mechanical engineering from the Budapest University of Technology and Economics (BME) in 1999 and 2002, respectively, and the D.Sc. degree from the Hungarian Academy of Sciences (MTA) in 2015.

He is currently an Associate Professor with the Department of Applied Mechanics, BME. Since 2016, he has been the Leader of the MTA-BME Lendület Human Balancing Research Group. His current research interests include time-periodic and time delay systems with applications on machine tool vibrations and human controlled systems.

Gábor Orosz received the M.Sc. degree in engineering physics from the Budapest University of Technology and Economics, Budapest, Hungary, in 2002, and the Ph.D. degree in engineering mathematics from the University of Bristol, Bristol, U.K., in 2006.

He held the post-doctoral positions with the University of Exeter, U.K., and with the University of California at Santa Barbara, Santa Barbara, CA, USA. In 2010, he joined the University of Michigan, Ann Arbor, MI, USA, where he is currently an Associate Professor of mechanical engineering. His research interests include nonlinear dynamics and control, time delay systems, and networks and complex systems with applications on connected and automated vehicles and biological networks.